The Broadband Radiative Properties of Cirrus Clouds Deduced from Aircraft Measurements During FIRE

by William L. Smith, Jr. and Stephen K. Cox

FIRE Series No. 7

Funding Agencies: National Aeronautics and Space Administration and Office of Naval Research

Colorado State University

DEPARTMENT OF ATMOSPHERIC SCIENCE

PAPER NO.
448

THE BROADBAND RADIATIVE PROPERTIES OF CIRRUS CLOUDS DEDUCED FROM AIRCRAFT MEASUREMENTS DURING FIRE

FIRE Series No. 7

by
William L. Smith, Jr.
and
Stephen K. Cox

Department of Atmospheric Science
Colorado State University
Fort Collins, CO 80523

October, 1989

Atmospheric Science Paper No. 448

ABSTRACT

THE BROADBAND RADIATIVE PROPERTIES OF CIRRUS CLOUDS DEDUCED FROM AIRCRAFT MEASUREMENTS DURING FIRE

The bulk radiative and microphysical properties of five cirrus clouds sampled via the NCAR Sabreliner on four days during the FIRE first cirrus IFO are described. These cirrus systems, which developed under a variety of synoptic weather conditions, occurred at various altitudes and ranged in geometric thickness from about 2.0 to 4.5 km. A broadband, infrared radiative transfer model is employed to deduce the impact of the cirrus layers on infrared radiation. This model isolates the effect of the atmospheric gases from that of the cloud ice water permitting retrieval of the cloud emittance (ϵ_{cld}) and profiles of the mass absorption coefficient (K).

For the five cirrus cloud cases, the total cloud emittance, ϵ_{cld}, ranged from about 0.4 to 0.8 and the deduced emittance profiles appear as similar functions of ice water path (IWP). Furthermore, the mass absorption coefficient, K, is found to decrease with increasing particle size ranging from about 0.48 m^2g^{-1} in the top of one layer to about 0.007 m^2g^{-1} near the base of another. This relationship is somewhat dissimilar from one cirrus system to the next suggesting the significant effect of some unmeasured microphysical property. Small particles, which have been shown by other authors to be prevalent in cirrus clouds via the spectral characteristics remotely sensed in the 8-12 μm window region, are a likely suspect. Broadband, infrared absorption coefficients (σ) are also computed and found to exhibit a similar temperature dependence as data recently presented by other authors.

The horizontal variabilities in the shortwave and infrared properties of these cirrus systems are explored. The range of variation in the shortwave properties are found to be

similar to the observed range in the infrared. Good correlation was found between the shortwave albedo (ρ) and upward effective emittance ($\epsilon^* \uparrow$). A scatter plot of these two parameters agreed well with theoretical calculations assuming an asymetry parameter of 0.7. Downward effective emittances ($\epsilon^* \downarrow$) were found to range from about 0.4 to 0.8, while the shortwave effective extinction (ς) ranged from 0 to 0.45. $\epsilon^* \downarrow$ and ς were not well correlated owing to cloud heterogeneities.

Finally, the current state of cirrus radiation parameterizations was briefly assessed in relation to this data set and there appears to be sufficient observational evidence to support the initial development of parameterization schemes for general circulation and climate models.

ACKNOWLEDGEMENTS

We thank Dr. Andrew Heymsfield and Karen Miller for providing the reduced microphysics data and NCAR's Research Aviation facility for acquisition of the Sabreliner data. We are also grateful to Ms. Melissa Tucker for her help in preparing this manuscript and to Paul Hein for his assistance concerning the Sabreliner data set. This research has been supported by the National Aeronautics and Space Administration Grant NAG 1-554 and by the Office of Naval Research Grant N00014-87-K-0228/P00002. Computer support and aircraft support were provided by the Scientific Computing Division and the Research Aviation Facility of the National Center for Atmospheric Research which is sponsored by the National Science Foundation.

CONTENTS

LIST OF FIGURES

LIST OF TABLES

Chapter 1

INTRODUCTION

It is well known that clouds are significant factors in weather and climate because of their effects on the radiation field and thus on the energy balance of the earth-atmosphere system. As a result, the accurate prediction of weather and climate depends to a significant degree on the accuracy with which cloud-radiation interactions can be described.

Recently, cirrus clouds have been the focus of numerous scientific investigations because of their importance to the earth-atmosphere climate system. Ramanathan, *et al.*, (1983), Randall, *et al.*, (1989) and others have indicated that the accurate representation of the radiative effects of cirrus clouds in general circulation models (GCMs) is critical to the accuracy with which the earth's climate may be simulated and/or predicted. Several theoretical investigations of the infrared radiative properties of cirrus clouds have been reported. Hunt (1973) and Liou (1974) conducted detailed investigations of the radiative properties of cirrus clouds in the atmospheric window region. Stephens (1980) presented 11μm and broadband radiative transfer calculations through cirrus. Recent advances in remote sensing by lidar and the availability of high altitude research aircraft have provided opportunities to study the radiative characteristics and microphysical composition of cirrus, in the hope that we may better understand these clouds which have been identified to be one of the major unsolved components in weather and climate research (Bretherton and Suomi 1973). Griffith, *et al.*, (1980) reported aircraft measurements of the radiative properties and microphysical composition of cirrus observed in the tropics during GATE, as did Paltridge and Platt (1981) for cirrus over New Mexico. Platt, *et al.*, (1987) reported the optical properties of midlatitude and tropical cirrus from a year's extensive LIRAD (developed by Platt, 1973) observations. Platt and Harshvardhan (1988) used LIRAD

results and the results of Heymsfield and Platt (1984) to investigate the sensitivity of climate to cirrus clouds. A comprehensive ground based experiment focusing on the radiative and optical properties of cirrus has been conducted in the Soviet Union (Abakumova *et al.*, 1989). During the Fall of 1986, the first Cirrus Intensive Field Observations (Cirrus IFO) was conducted in Wisconsin. This IFO is a major component of the First ISCCP (International Satellite Cloud Climatology Project) Regional Experiment (FIRE) (Cox *et al.*, 1987)

It is the purpose of this investigation to report the broadband radiative and microphysical properties of several cirrus systems, as observed from the NCAR Sabreliner during the FIRE first Cirrus IFO, in order to better understand cirrus cloud-radiation interactions. A broadband infrared (BBIR) radiative transfer model is employed to deduce BBIR absorption coefficients in order to assess the impact of the cirrus clouds on infrared radiation. The relationships of these absorption coefficients to temperature and microphysical characteristics are explored. The horizontal variabilities observed in the BBIR and broadband shortwave (BBSW) radiative properties are presented and compared. Finally, the current state of cirrus cloud radiation parameterizations is assessed in relation to this new data.

Chapter 2

ANALYSIS METHODS

2.1 Broadband Infrared Radiative Transfer Model

In order to assess the impact of the cloud layers on infrared radiation, the broadband (4-50 μm) irradiance data were analyzed utilizing a broadband infrared radiative transfer model similar to that described by Cox and Griffith (1979). For clear sky, this model is capable of reproducing broadband divergence values which agree with observations (Albrecht, *et al.*, 1974). The integral emittance values of the three radiatively important gases, H_2O, CO_2 and O_3 were calculated from an integral transmission approximation which, in the absence of scattering, is given by

$$\epsilon(T, p_o, p)_i = \frac{\int_{\lambda_1}^{\lambda_2} B(\lambda, T)[1 - \mathcal{T}(\lambda, u[p_o, p], T)]d\lambda}{\int_0^{\infty} B(\lambda, T)d\lambda}, \tag{2.1}$$

where $\mathcal{T}$ is the spectral transmittance for a layer bounded by the reference pressure p_o and pressure p containing the optical mass $u(p_o, p)_i$ of the appropriate optically active constituent. The index i represents the spectral band pass $\lambda_1 - \lambda_2$. $B(\lambda, T)$ is the Planck function where T represents temperature and λ represents wavelength. A list of the spectral bandpasses over which Eqn. (2.1) was evaluated and the sources of the spectral transmittance data are given in Cox and Griffith (1979).

Infrared irradiance values as a function of pressure were calculated from the infrared emittance values and atmospheric temperature and moisture profiles obtained from the nearest radiosonde soundings. The temperature profiles through the cirrus clouds were taken from the aircraft measurements and were found to be within 0.5°C of the radiosonde data. CO_2 was assumed to be uniformly mixed with a constant mixing ratio of .501 g/kg.

The ozone mixing ratio profile and the temperature and moisture profiles above the highest radiosonde observation were obtained by averaging the summer and winter midlatitude profiles from McClatchey, *et al.*, (1972). Due to instrument limitations, accurate absolute humidity measurements were not made at frost point temperatures less than −54°C. For this reason, our analysis was conducted for two assumed profiles of water vapor mixing ratio within the cloud layers. The first profile was constructed assuming that the entire cloud was saturated with respect to ice. The second profile was constructed using measurements from the frost point hygrometer at frost point temperatures (T_f) greater than -54°C and data from the Lyman alpha absorption hygrometer at temperatures less than -54°C, since the frost point hygrometer fails to respond to humidity changes in this regime. Because no absolute calibration was available for the Lyman alpha data, it was calibrated against the frost point hygrometer data at $T_f > -54$°C and this curve was extrapolated to fit the Lyman alpha measurements at $T_f < -54$°C. The assumed water vapor mixing ratio profiles for 28 October and 31 October are shown in Figs. 2.1 and 2.2 Although their is some degree of uncertainty in the way the measured water vapor profiles were obtained, these profiles may be more realistic than assuming ice saturation considering the tenuous nature of the cirrus clouds observed on these four days. For this reason, the results presented in Chapter 3 were obtained using the measured water vapor profiles.

With the exception of the treatment of cloud, the basic computational technique is identical to that of Griffith, *et al.*, (1980) where the irradiance at a pressure level p is given by Eqn. (2.2) assuming a plane parallel atmosphere in local thermodynamic equilibrium and neglecting scattering.

$$H(P_i) = \underbrace{\int_{P_o}^{P_i} B(T,p)\frac{\partial \epsilon_g}{\partial p}dp}_{A} + \underbrace{H_o\left[1 - \int_{P_o}^{P_i}\frac{\partial \epsilon_g}{\partial p}dp\right]}_{B} \tag{2.2}$$

$$+ \underbrace{\int_{P_o}^{P_i} B(T,p)\left(\frac{\partial \epsilon_{cld}}{\partial p} - \frac{\partial \epsilon_{ovl}}{\partial p}\right)dp}_{C}$$

$$+ \underbrace{H_o\left[1 - \int_{P_o}^{P_i}\left(\frac{\partial \epsilon_{cld}}{\partial p} - \frac{\partial \epsilon_{ovl}}{\partial p}\right)dp\right]}_{D}$$

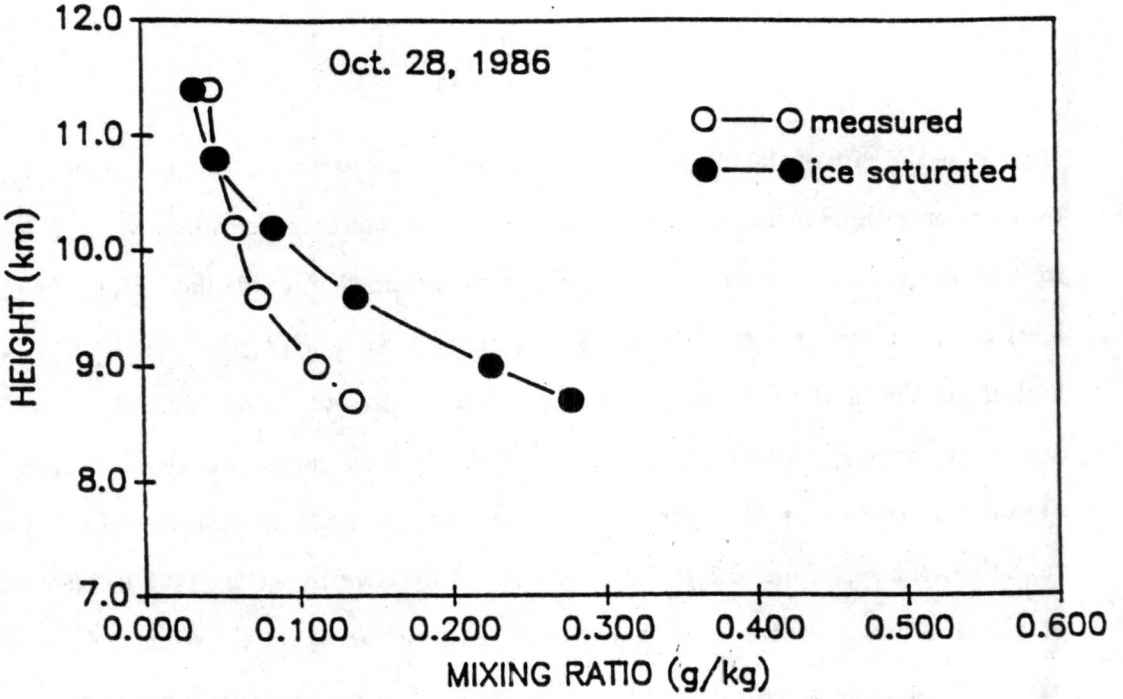

Figure 2.1: Vertical profiles of water vapor mixing ratio for October 28, 1986.

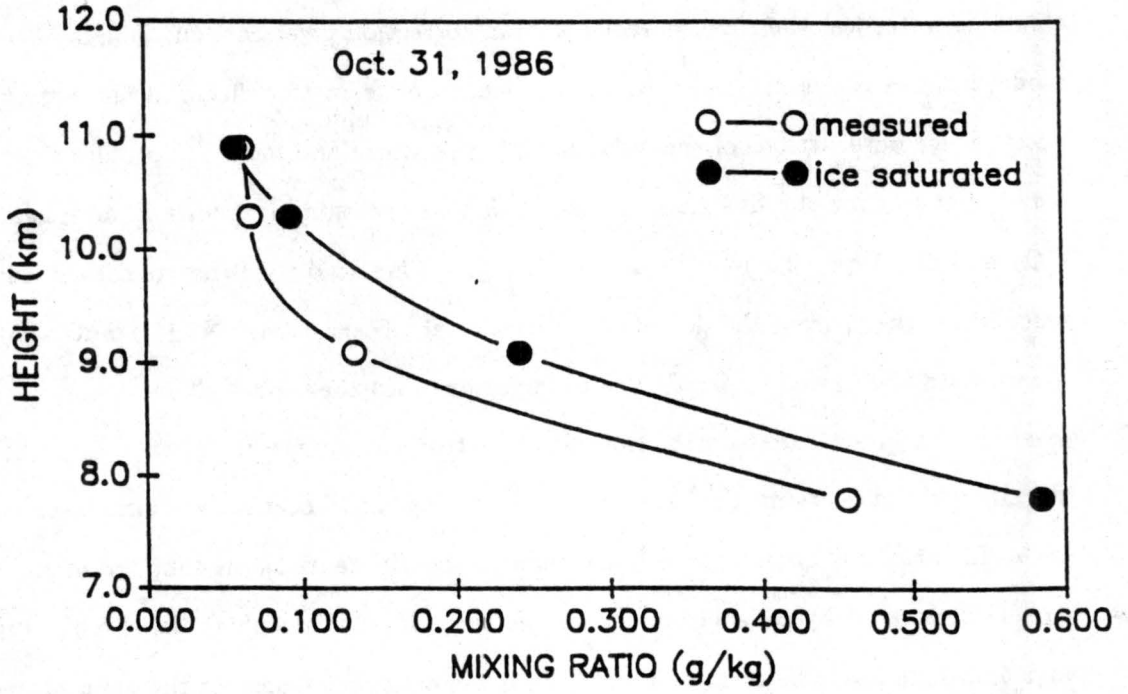

Figure 2.2: Vertical profiles of water vapor mixing ratio for October 31, 1986.

where

$$\frac{\partial \epsilon_{ovl}}{\partial p} = \frac{\partial (\epsilon_g \cdot \epsilon_{cld})}{\partial p} \quad . \tag{2.3}$$

Here, ϵ_g is the sum of the integral flux emittances of the atmospheric gases minus a gaseous overlap correction in the column extending from the reference pressure level p_o (i.e. $p_o = 0$ for the downwelling calculation and $p_o = p_{sfc}$ for the upwelling calculation), to the pressure level p, ϵ_{ovl} is the grey cloud-gaseous overlap correction, $B(T,p)$ is the Planck function and H_o is the emitted irradiance at the reference pressure level (i.e. $H_o(p_o = 0) = 0$ and $H_o(p_o = p_{sfc}) = \sigma T_{sfc}^4$). The form of the overlap correction given in Eqn. 2.3 is obtained by assuming that the product rule for transmittances applies for broadband radiative transfer. Eqn. 2.3 has been employed by Griffith, *et al.*, (1980), Ramanathan, *et al.*, (1983) and others even though it is, at best, an approximation and no attempt has been made to assess its accuracy. However, it is particularly convenient because it ensures that ϵ_{cld} does not exceed 1.0. Terms A and B on the right-hand side of Eqn. 2.2 represent the power emitted and transmitted, respectively, by the atmospheric gases while Terms C and D represent the power emitted and transmitted, respectively, by the cloud ice water less the cloud-gaseous overlap correction given in Eqn. 2.3. In effect, this model isolates the emittance of the cloud ice water from the effects of the atmospheric gases. Since observations of the irradiance, temperature and moisture profiles were made simultaneously for the five cases presented here and assuming known concentrations of CO_2 and O_3, Eqn. 2.2 may be solved for ϵ_{cld}. This study will be concerned with the calculation of ϵ_{cld} from the downwelling irradiance observations. No attempt is made to incorporate the upwelling irradiance observations into the model. This is because lower level clouds, unmeasured by the Sabreliner instrumentation, were often present beneath the cirrus cloud decks in each case except 28 October and because ϵ_{cld} is more sensitive to the differential downwelling irradiance than to the differential upwelling irradiance. This can be illustrated by considering the simple three layer atmosphere depicted in Fig. 2.3 and approximating the form of Eqn. 2.2 for a single constituent of the atmosphere (i.e. gas or cloud) by

$$H(P_i) = \sum_i \sigma T_i^4 \Delta\epsilon_i + H_o \left[1 - \sum_i \Delta\epsilon_i\right] \quad . \tag{2.4}$$

Thus, the downwelling irradiances at the first two levels beneath the upper boundary may be expressed as

$$H_1 \downarrow = \sigma T_1^4 \Delta\epsilon_1 \tag{2.5}$$

and

$$H_2 \downarrow = \sigma T_1^4 \Delta\epsilon_1 + \sigma T_2^4 \Delta\epsilon_2 \quad . \tag{2.6}$$

Similarly, the upwelling irradiance at the first two levels above the lower boundary may be written as

$$H_1 \uparrow = \sigma T_3^4 \Delta\epsilon_1 + H_o \left[1 - \Delta\epsilon_1\right] \tag{2.7}$$

and

$$H_2 \uparrow = \sigma T_2^4 \Delta\epsilon_1 + \sigma T_3^4 \Delta\epsilon_2 + H_o \left[1 - \Delta\epsilon_1 - \Delta\epsilon_2\right] \quad . \tag{2.8}$$

A similar expression may be written for $H_3 \downarrow$ but is not necessary for this discussion. In Eqns (2.5)-(2.8), T_1, T_2 and T_3 are the mean effective radiating temperatures of layers 1, 2 and 3, $\Delta\epsilon$ is the appropriate emittance increment, $H_o \downarrow = 0$ at the upper boundary and $H_o \uparrow = \sigma T_{sfc}^4$ at the lower boundary. Note that if each layer contains an equal amount of optical mass, then $\Delta\epsilon_1$ is the same for each irradiance calculation. The same is true for $\Delta\epsilon_2$. The emittance of this atmosphere with a temperature profile that is not isothermal can be shown to be more sensitive to the differential downwelling irradiance than to the differential upwelling irradiance by considering that for layer 2,

$$\Delta H \downarrow = H_2 \downarrow - H_1 \downarrow = \left(\sigma T_2^4 - \sigma T_1^4\right) \Delta\epsilon_1 + \sigma T_1^4 \Delta\epsilon_2 \tag{2.9}$$

and

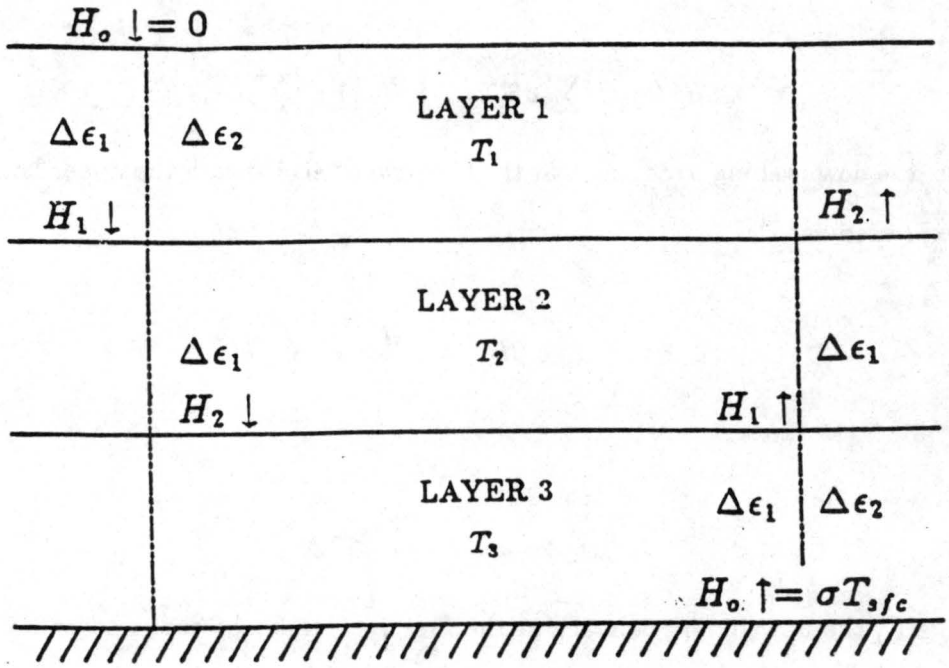

Figure 2.3: Schematic illustrating the simplified sensitivity of irradiance to emittance for a 3-layer atmosphere where each layer contains an equal increment of optical mass.

$$\Delta H \uparrow = H_2 \uparrow - H_1 \uparrow = -\left(\sigma T_0^4 - \sigma T_3^4\right) \Delta\epsilon_2 - \left(\sigma T_3^4 - \sigma T_2^4\right) \Delta\epsilon_1 \ . \qquad (2.10)$$

Since the second term on the rhs of Eqn.(2.9) is considerably larger than the other terms in Eqns.(2.9) and (2.10), $\Delta H \downarrow$ will be more sensitive than $\Delta H \uparrow$ to the emittance.

2.1.1 Model Application

The broadband infrared radiative transfer model results for a clear sky atmosphere on 31 October are shown in Fig. 2.4 for the downwelling radiation. Also shown are the measured irradiances in a cirrus cloud. The highest measured irradiance shown was made in clear sky just above the cloud top. The apparent discrepancy between the calculated and the measured irradiance at cloud top (clear sky) occurred for all four cases. Table 2.1 lists the difference in calculated and measured irradiance for each of the four cases described here. In each case, the measurement is significantly higher than the calculation These discrepancies are similar in magnitude and are most likely due to a combination o the following:

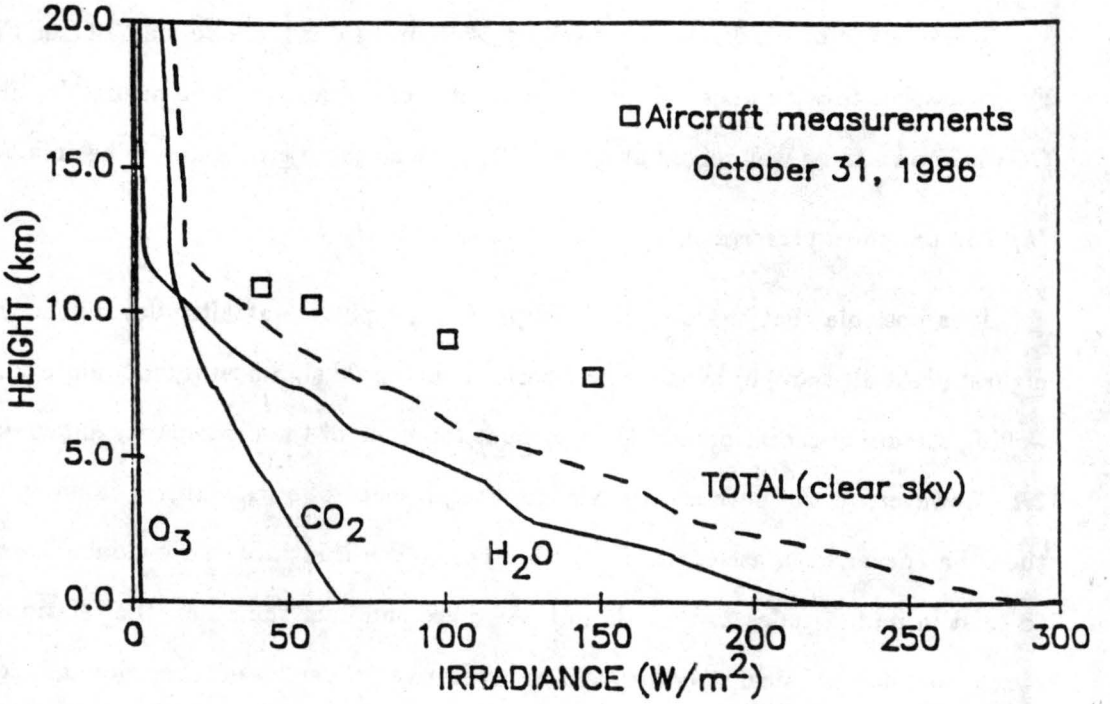

Figure 2.4: Profiles of H_2O vapor, CO_2, O_3 and the total clear sky calculated irradiance versus aircraft irradiance measurements made on October 31, 1986.

(1) Uncertainties in the specified temperature and gaseous profiles

Errors due to uncertainties in the specified temperature and gaseous profiles are expected to be less than 3 Wm^{-2} for the calculation of downwelling irradiance at levels near the tropopause. Random errors in the temperature and moisture profile above cloud top were applied to the case of 31 October. Assuming a normal distribution with a standard deviation of 1.0°C, the temperature profile was randomly perturbed for ten model runs. The calculated irradiances at cloud top were within 1 Wm^{-2}. Similarly, the water vapor profile was randomly perturbed assuming errors as large as 10% in the summer-winter average midlatitude water vapor profile from McClatchey, *et al.*, (1972). The calculated irradiances at cloud top were again within 1 Wm^{-2}. Errors could be as large as 6 Wm^{-2} assuming errors in water vapor mixing ratio as large as 100%, however this is highly unlikely since water vapor concentrations above the tropopause do not change this significantly from day to day during the Fall in midlatitudes.

The effect of ozone on the downwelling 4-50 μm irradiance is very small (see Fig. 2.4) Errors associated with uncertainties in the profile of ozone should be negligible. Similarly CO_2 is known to be well mixed at about .501 g/kg so these errors should be small as well.

(2) The unknown presence of upper tropospheric clouds

It is possible that the presence of upper tropospheric (at altitudes higher than the highest flight altitude) or even stratospheric clouds could significantly modulate the downwelling stream of radiation and thus account for some of the discrepancy shown in Table 2.1. However, to the author's knowledge, the presence of stratospheric cloud in midlatitudes has never been ascertained. Furthermore, even if stratospheric clouds were known to exist in midlatitudes as they do in the tropics and over the poles, the relationship between the microphysical structure and the radiative properties of these clouds is relatively unknown. In some instances (i.e., 31 October), observers on board the Sabreliner noted very thin cirrus, in the local vicinity, at altitudes above the altitude ceiling of the aircraft (about 12 km). However, in most cases, extremely clear conditions were noted above the cirrus cloud tops. Based on this knowledge, or lack thereof, the existence of some form of subvisible cirrus at and above the tropopause during all four flights, in which similar discrepancies between the calculated and measured clear sky irradiance occurred, seems unlikely.

(3) Inaccuracies in the absolute measurement of irradiance

Inaccuracies in the absolute measurement of irradiance may occur due to poor calibration of the Eppley pyrgeometers. Calibration techniques for the pyrgeometer have been described by Albrecht and Cox (1976,1977). There is evidence that one of the calibration constants was not properly determined in the laboratory via one of these techniques. It is estimated that this could be responsible for up to 7 or 8 Wm^{-2} of the discrepancy shown in Table 2.1.

(4) Errors due to the approximations and assumptions used in developing the model physics

Table 2.1: Measured Minus Calculated Clear Sky Irradiance at Cloud Top

Date	Height (km)	Measured-Calculated Irradiance (Wm^{-2})
October 19, 1986	11.0	15.8
October 22, 1986	11.9	13.0
October 28, 1986	11.4	11.0
October 28, 1986	10.8	13.5
October 31, 1986	10.4	10.2

It is, of course, possible that the discrepancies shown in Table 2.1 arise because of inaccuracies in the model physics. The broadband infrared (BBIR) radiative transfer model described above represents an approximate solution to the very detailed and complex radiative transfer equation. As stated previously, this model has been shown to accurately reproduce broadband divergence values in clear sky. A preliminary comparison between the BBIR radiative transfer model and LOWTRAN7 calculations of clear sky downwelling flux near the surface yielded values within 3%, remarkably good considering the simplifications in the BBIR model physics. Clear sky downwelling fluxes at about 12 km calculated from these two models were also compared and found to be within 2.5 Wm^{-2} (within 10 %). Thus, it is likely that the discrepancies shown in Table 2.1 are not due to problems with the model physics but rather due to one or more of the possible explanations stated above.

2.1.2 Parameterization of Cloud Emittance

We have chosen to treat the cloud as a greybody where

$$\epsilon_{cld} = 1 - e^{-\tau_{cld}} \tag{3}$$

and

$$\tau_{cld} = \sum_i (K_i \cdot \overline{IWC}_i \cdot \Delta Z_i) = \sum_i \sigma_i \cdot \Delta Z_i \cdot \tag{4}$$

In (4), K_i is the greybody mass absorption coefficient, $\overline{IWC_i}$ is the mean ice water content, σ_i is the broadband absorption coefficient (units m^{-1}) and ΔZ_i is the thickness for the i^{th} cloud layer. Paltridge (1974) and Stephens (1978) have shown that when employing a constant value of K, (4) is a good descriptor of the radiative properties of water clouds. Griffith, *et al.*, (1980) successfully employed this relationship, assuming a constant value of K, to fit irradiance observations of cirrus obtained during GATE, although to date, there is no theoretical basis supporting the assumption that the broadband cloud transmittance through cirrus is truly an exponential function of optical depth. Therefore, we have adopted (4), but with the assumption that K may be variable through the cirrus layer. This parameterization of cloud emittance permits us to retrieve profiles of K that yield calculated irradiance profiles that precisely match the measured irradiance profiles through the cirrus clouds.

Platt and Harshvardhan (1988), hereafter referred to as PH, discuss the relationship between cirrus cloud absorption and ice water content and provide insight into why the mass absorption coefficient, K, may not be a constant through a cirrus cloud of variable ice particle size distribution. As in PH, K may be considered as:

$$K = \frac{\sigma}{IWC} \simeq \beta \frac{\overline{Q}_a}{r_e} , \tag{5}$$

where $\overline{Q}_a$ is the "effective absorption efficiency," r_e the "effective radius" for the size distribution and β is a constant which includes the density of ice and an ice particle orientation factor. Theoretical computations of the absorption efficiency Q_a (or extinction efficiency) as a function of size parameter have been carried out by Herman (1962), Pinnick, *et al.*, (1979) and others. For incident energy in the infrared wavelengths, $\overline{Q}_a \approx c \cdot r_e$ (c is some constant) for size parameters typically found in fogs and stratiform water clouds and thus K is approximately constant. However, for ice clouds where typical ice crystal dimensions are known to be an order of magnitude larger than the water droplet dimensions found in stratiform clouds, the absorption efficiency approaches a value of unity so that K cannot be treated as a constant through cirrus unless r_e remains constant. This is clearly not the case for the cirrus clouds observed during the FIRE first cirrus IFO. Fig.

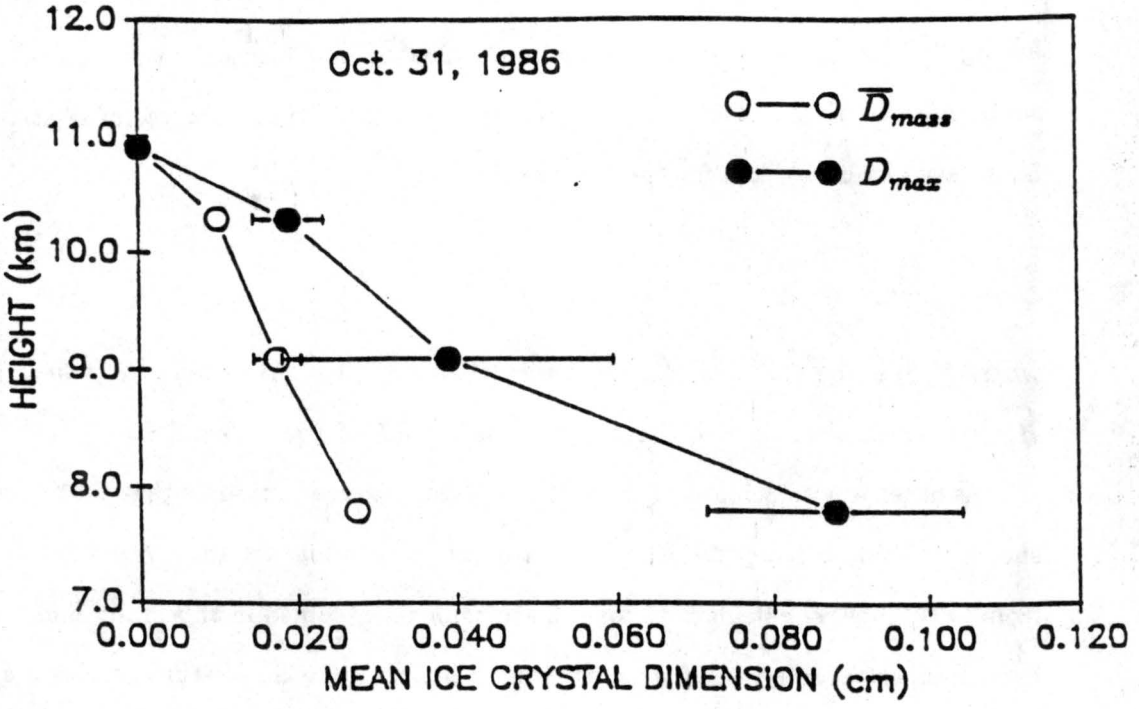

Figure 2.5: Vertical profile of mean ice crystal dimension for the cirrus cloud sampled on October 31, 1986. See text for description of the parameters $\overline{D}_{mass}$ and D_{max}.

2.5 shows the parameters $\overline{D}_{mass}$ and D_{max} varying as a function of height for the cirrus cloud sampled on 31 October. $\overline{D}_{mass}$ is the median mass weighted ice particle dimension and D_{max} is the mean maximum dimension (Heymsfield and Miller, 1989). Similar figures are shown for the other four cirrus cloud cases in Appendix A. In Section 3.1.2, the nature of the relationship between K and particle dimension is explored.

2.1.3 Normalization at Cloud Top

In order to accurately retrieve ϵ_{cld}, as described above, agreement between the measured and calculated downwelling irradiance at the cloud top is essential. As discussed in the previous section, this agreement is not realized and must be forced computationally. Griffith, *et al.*, (1980) forced the calculated downwelling irradiance to match the measured irradiance by iteratively adjusting the background flux H_o of Eqn. 2.2. Although there is no physical basis for $H_o(P = 0) \neq 0$, it ensures that the calculation is adjusted as far away from the cloud boundary as possible, thus minimizing the effect of the adjustment on the retrieval of ϵ_{cld} and K. The exact value of H_o necessary to ensure agreement at the cloud boundaries may be obtained from one model run under clear sky conditions by

saving the gaseous emittance information evaluated in the integrals of Eqn. 2.2. After some manipulation, the exact H_o adjustment which will ensure agreement at the cloud boundary can be written for the downwelling calculation as

$$H_o^{adj} = \frac{H_c^m}{H_c^c - 1} \cdot \frac{A}{1 - E} \quad , \tag{6}$$

where H_o^{adj} is the adjusted H_o, H_c^c is the calculated clear sky irradiance (where $H_o = 0$), H_c^m is the measured clear sky irradiance, A is Term A of Eqn. 2.2 and E is $\int_{P=0}^{P=P_{cldtop}} \frac{\partial \epsilon_g}{\partial p} dp$.

Another way to achieve agreement at the cloud top is to assume that the discrepancies shown in Table 2.1 are due mainly to a measurement bias by the pyrgeometer. Results from LOWTRAN7 calculations for the atmospheres assumed in this study and integrated over the spectral response of the pyrgeometer indicate that an instrument bias is a distinct possibility since the clear sky flux calculations of LOWTRAN7 and the BBIR radiative transfer model agree quite well. The strategy applied here was to adjust each measurement of the irradiance profiles by an amount that would equate the measurement at cloud top to the calculation (i.e. by the appropriate amount listed in Table 2.1). Although, the adjustment of the background flux is now unnecessary (so that $H_o(P = 0) = 0$), this method may suffer in accuracy from the assumption that the instrument bias is a constant at different altitudes. Fig. 2.6 shows the two assumed profiles for the case of 31 October along with the clear sky calculation. The circles are the actual measurements and the triangles represent an adjusted profile assuming a measurement bias that is constant with height so that the clear sky calculation agrees with the measured flux at cloud top.

The model was run for both profiles and for a similar set of profiles from each flight in order to compare the effects of these two strategies on the retrieval of ϵ_{cld} and K. Fig. 2.7 shows the resulting K values for these two strategies and a similar comparison is shown in Fig. 2.8 for ϵ_{cld}. The values of ϵ_{cld} and K are about 10% higher for the case where H_o is adjusted. There are two factors which may contribute to this difference. One concerns the effect of assuming $H_o \neq 0$ in the calculation of downwelling irradiance, while the other may be appreciated by considering two profiles of irradiance (i.e. Fig 2.6) each with

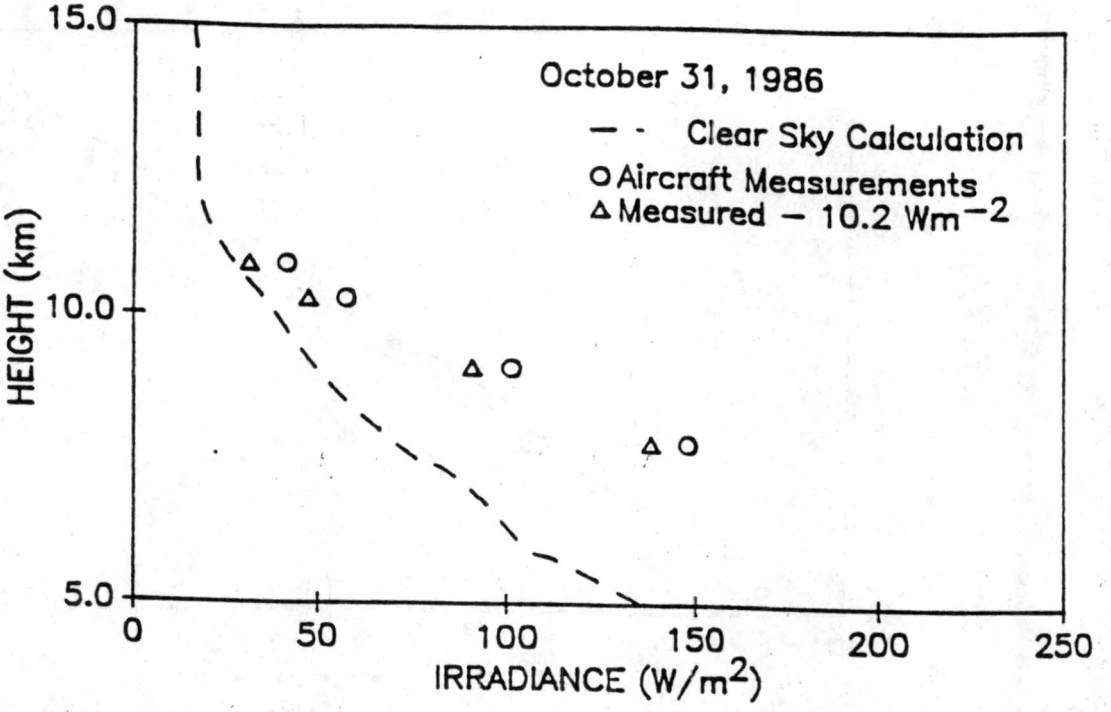

Figure 2.6: Clear sky irradiance calculation versus the aircraft irradiance measurements and the measurements adjusted by a 10.2 Wm^{-2} bias.

the identical vertical slope but offset from each other. The downward effective emittance ($\epsilon^* \downarrow$) may be calculated directly from these irradiance profiles since

$$\epsilon^* \downarrow = \frac{H_B \downarrow - \overline{H}_T \downarrow}{\sigma \overline{T}^4 - \overline{H}_T \downarrow}. \tag{7}$$

Here, $H \downarrow$ denotes downwelling infrared irradiance, the subscript T indicates incidence at the cloud top and the subscript B denotes incidence at some level below cloud top. For the purpose of this section, the temperature T is taken to be the mean temperature of the layer between the cloud top and the level B. The effective emittance will be discussed further in Section 2.3. From Eqn. 7, one can determine that $\epsilon^* \downarrow$ will be larger for the profile with the larger values of irradiance than for the other profile. Furthermore, ($\epsilon^* \downarrow$) may be linearly related to ϵ_{cld} as Fig. 2.9 suggests. This implies, among other things, that the appropriateness of adjusting H_o to achieve agreement at the cloud top may be explored. The exact linear relationship between ϵ_{cld} and ϵ^* was determined for the irradiance profile comprised of triangles in Fig 2.6 because the adjustment of H_o was not necessary for the retrieval of ϵ_{cld}. This relationship was used to estimate values of ϵ_{cld}

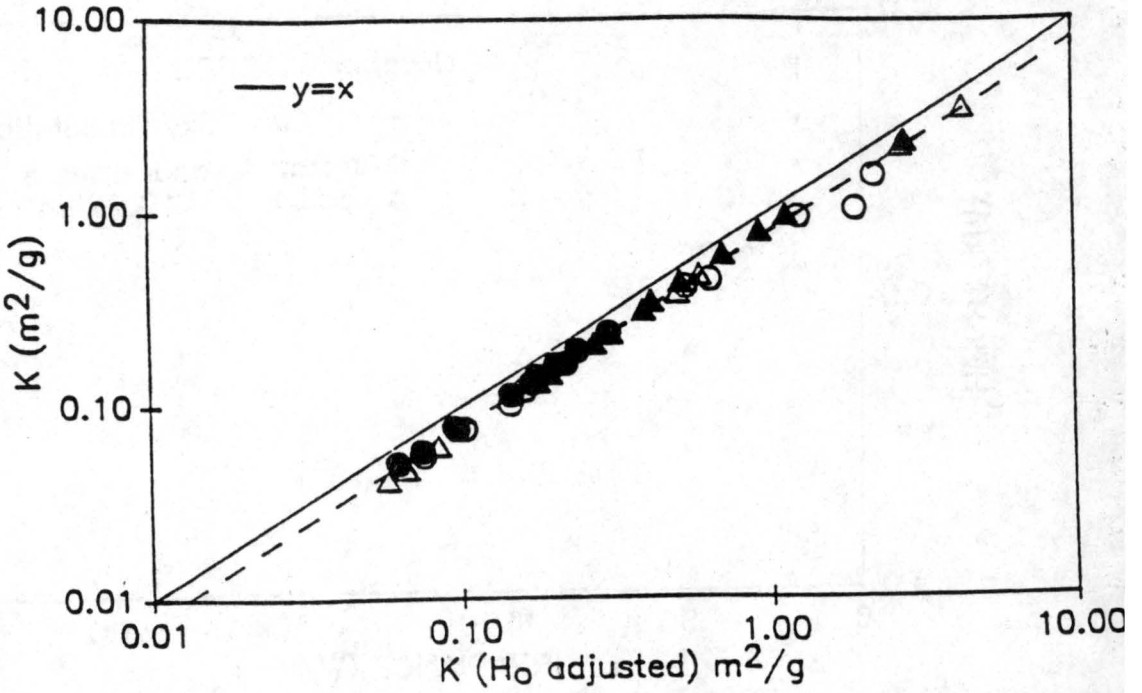

Figure 2.7: Retrieved mass absorption coefficients (K) deduced from the irradiance obser vations with an applied 10.2 Wm^{-2} bias versus those deduced from the actual measure ments where H_o was adjusted.

from the ϵ^* values computed for the other irradiance profile (circles) in Fig. 2.6. Give that the relationship between ϵ_{cld} and ϵ^* is linear, this new set of values for ϵ_{cld} shoul correspond to those values that would be retrieved by the model for the larger irradianc profile (circles) under the condition that the calculated and measured clear sky irradiance agree at the cloud top. A close comparison of these values to those actually retrieved b the model for the larger irradiance profile (circles) (where, in this case, the adjustment o H_o was necessary to force agreement at the cloud top) revealed agreement within 2.5% This implies that adjusting H_o to force an agreement between the calculated and measure clear sky irradiances at cloud top has a relatively small effect on the accurate retrieval o ϵ_{cld}, and thus K.

In summary, it appears that the accuracy with which ϵ_{cld} and K can be retrieved b incorporating irradiance observations into the radiative transfer model described abo depends on the accuracy of the irradiance observations. For this study, it was assume that there was no instrument bias so that the measured irradiances represent the actu irradiance profile. Therefore, the discrepancies between the measurements and calculatio

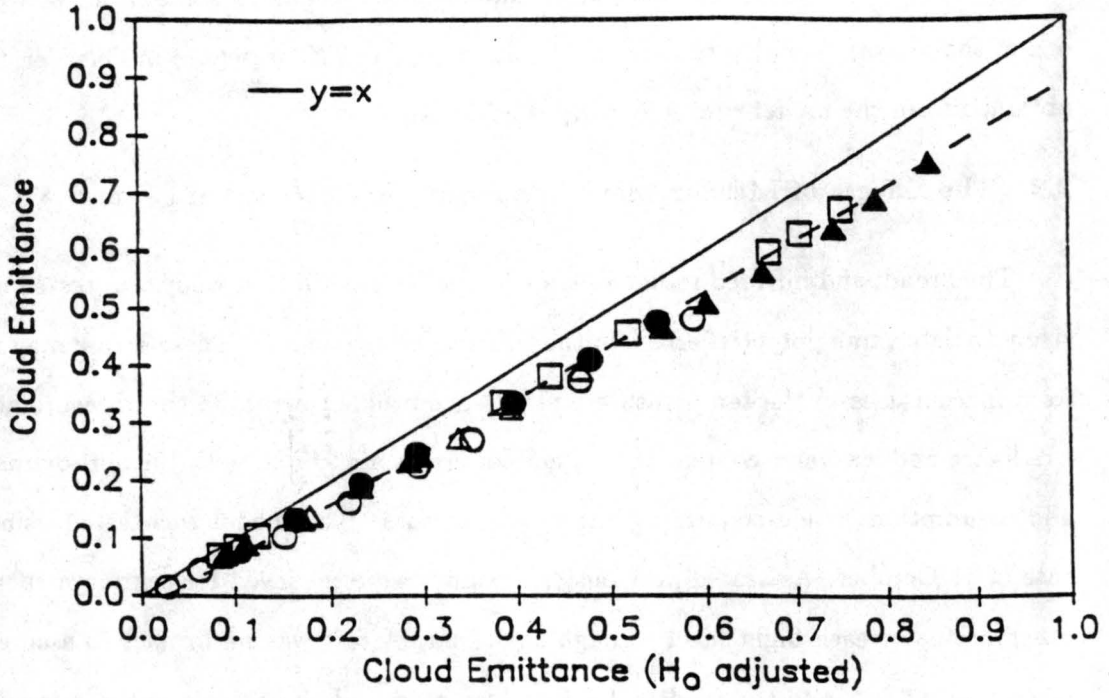

Figure 2.8: Same as Fig. 2.7 but for ϵ_{cld}.

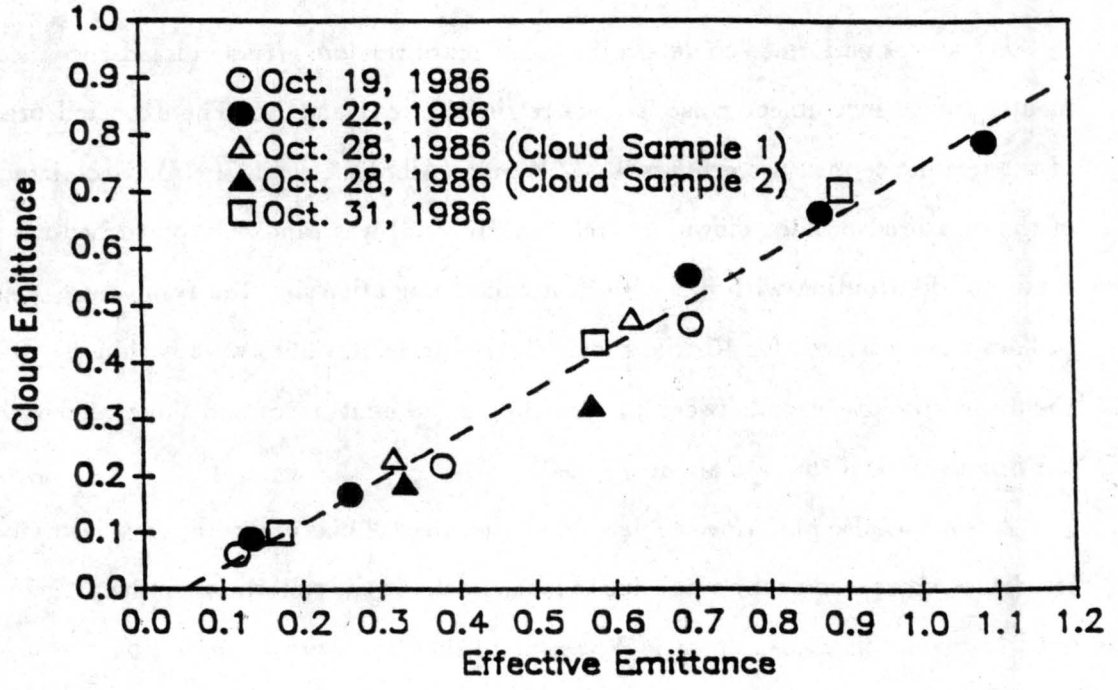

Figure 2.9: Model deduced cloud emittance (ϵ_{cld}) versus the observed effective emittance ($\epsilon^* \downarrow$) for five cirrus clouds. Here, $\epsilon^* \downarrow$ was computed using the layer mean temperature.

of irradiance at cloud top (Table 2.1) are assumed to be due to some other factor (i.e. one of the above). For this reason, the results of ϵ_{cld} and K presented in Chapter 4 were obtained from the model runs where H_o is adjusted.

2.2 The Effects of Measurement Errors on the Retrieval of ϵ_{cld} and K

The broadband infrared radiative transfer model used in this study was tested extensively to determine potential errors in the retrieval of ϵ_{cld} and K. These errors may result from inaccuracies in the temperature and gaseous profiles, errors in the measurement of irradiance and ice water content (IWC) and/or errors associated with the approximations and assumptions made concerning the model physics. The model was tested using the case of 31 October. As stated previously, K values were retrieved for each layer between observations at each flight level through the cloud. A test was performed to assure that when used as input to the model, the K values produced the exact measured irradiance profile.

2.2.1 The Effects of Errors in Irradiance Measurements

A test was performed to determine the effect of random errors in irradiance measurements, due to instrument noise, on the retrieval of ϵ_{cld} and K. The expected precision of the irradiance measurements is +/- 2 Wm^{-2} (Albrecht, et al., 1974). Each irradiance of the measured profile (shown as circles in Fig. 2.6) was randomly perturbed assuming a normal distribution with a 2 Wm^{-2} standard deviation and the resulting ϵ_{cld} and K profiles were retrieved for 10 trial runs. The resulting K values were within +/- 9% and the mean absolute error between the resulting cloud emittances and those retrieved from the original model run was about +/- 0.01.

A test was also performed to determine the effect of bias errors in the measurement of irradiance. Bias errors may occur due to inaccuracies in the calibration of the pyrgeometers used to make this measurement. We estimate that these errors should be within +/- 5 Wm^{-2}. Positive and negative biases were applied to the measured irradiance profile of 31 October. Figs. 2.10 and 2.11 depict the effects of these biases on the retrieved K values and ϵ_{cld}, respectively. The resulting error in K for a +/- 5 Wm^{-2} bias is about 8% and

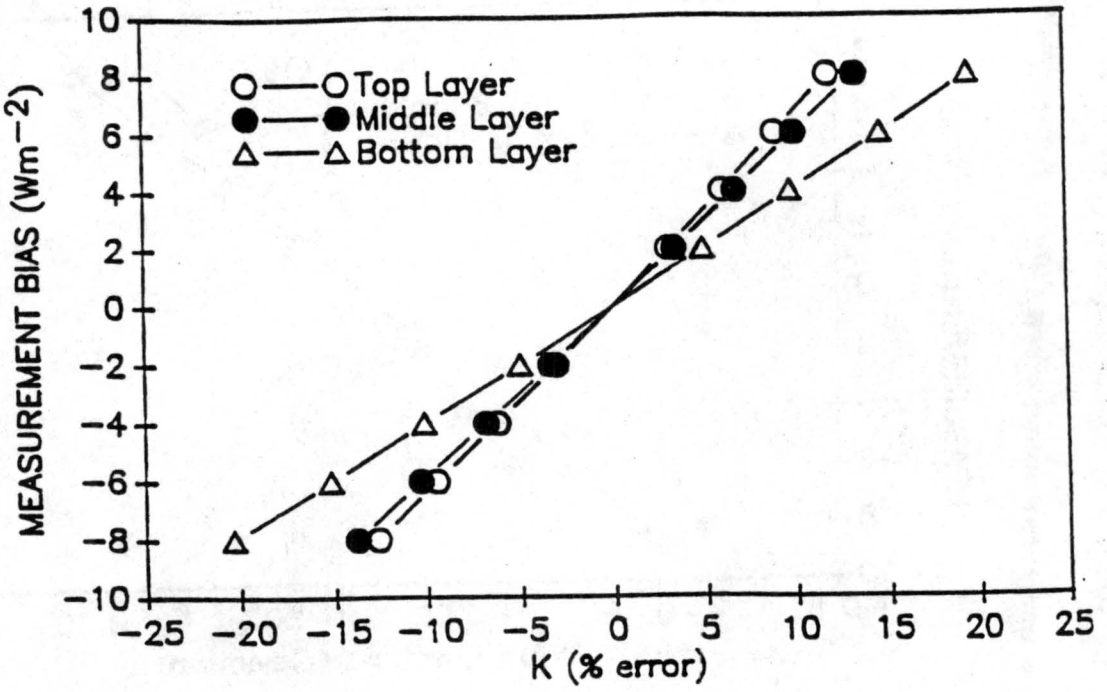

Figure 2.10: The effect of measurement biases in irradiance on the retrieval of the mass absorption coefficient (K).

the resulting error in the retrieved ϵ_{cld} is 0.02. Note that the errors increase with depth into the cloud. It is likely that as the integral in Eqn. 2.2 is solved at each level in the cloud, the error at that cloud level is amplified by errors in the calculation at the previous cloud levels.

Another potential source of error in the measured irradiance profiles arises due to the nonsteady state of the cloud field. Because only one aircraft was used to make measurements at different levels in the cloud, sampling errors may occur. In order to minimize these errors, some data were eliminated as discussed in Appendix A. In addition, we've adopted the analysis strategy described in Chapter 3.0 in order to set some limits on the observed radiative properties of the cirrus clouds.

Finally, a test was performed to determine if the relationship between the measured irradiance profile and the retrieved cloud emittance profile is linear such that

$$\epsilon(\overline{H}) = \overline{\epsilon(H)} \; . \tag{8}$$

The term on the left hand side (lhs) of the equality in Eqn. (8) is the cloud emittance profile retrieved from the mean irradiance profile. The term on the right hand side (rhs)

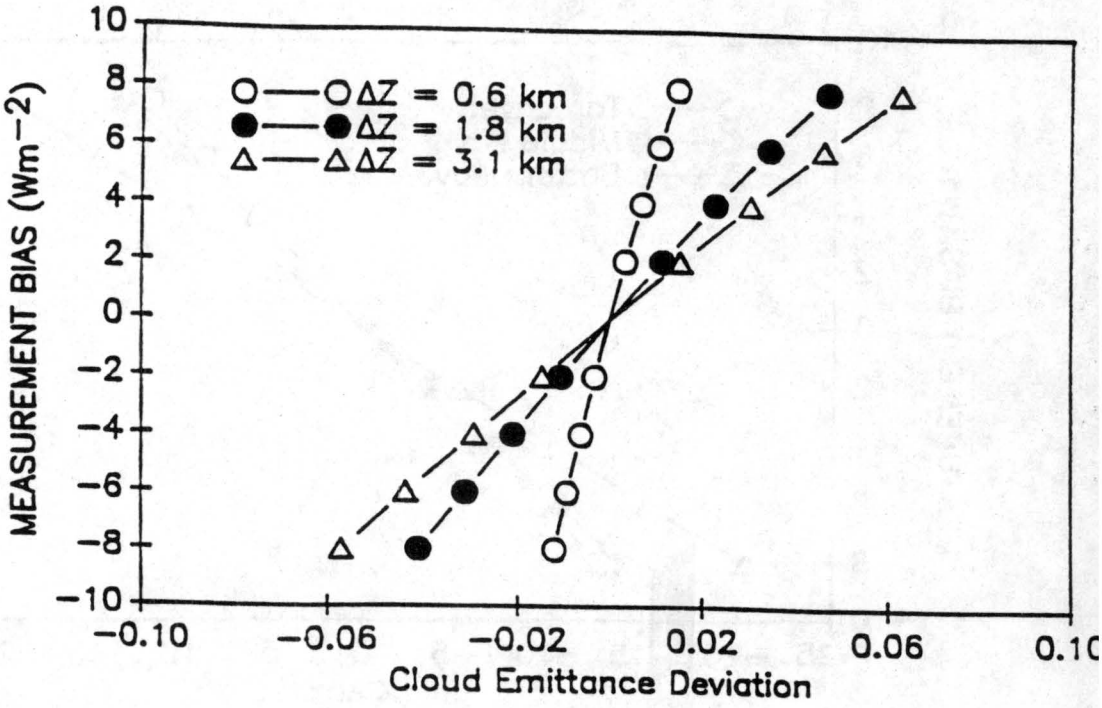

Figure 2.11: Same as Fig. 2.10 but for ϵ_{cld}.

is the average of the emittances retrieved from the combination of irradiances that mak up the mean ($\overline{H}$ on the lhs). To test the validity of Eqn. (8), ten irradiance profiles wer constructed. The mean irradiance at each level was calculated and a single emittanc profile was retrieved from the model. This represents the term on the lhs of Eqn. (8 Then, the emittance profile was retrieved from the model for each of the 10 irradianc profiles and averaged. This represents the rhs. of Eqn. (8). The results indicated tha Eqn. (8) is true to +/- .02%.

2.2.2 The Effects of Errors in Ice Water Content

The effect of errors in ice water content (IWC) on the retrieval of ϵ_{cld} and K w examined. Because IWC is not a directly measurable quantity, it is estimated from info mation obtained by the 2-D PMS probes flown on board the Sabreliner. The reductic of this data has been described by Heymsfield and Miller, 1989 (hereafter referred to HM) for the 28 October flight. For this case, the probe sized particles from about 44 μ to above 1.0 mm in 25 μm increments and particle habits were estimated from the 2- images (HM, 1989). The classification of particle habit from the 2-D images for the oth

three flights described here was automated based on the more selective criteria of the 28 October case (Andrew Heymsfield, personal communication). The effect of errors in IWC estimates on the retrieval of K will be equal and opposite since the quantity K times IWC is conserved in Eqn. (4). Thus, there will be no error in ϵ_{cld}. HM (1989) report that errors in IWC could be as large as 50%. If this is true, it follows directly that the K values are only accurate within a factor of 2.

2.2.3 The Effect of Errors in Temperature and Water Vapor Measurements

Because there is some degree of uncertainty in the temperature and moisture profiles obtained from the aircraft measurements, the model was tested to determine the effect of these errors on the retrieval of ϵ_{cld} and K. Errors in the measurement of temperature are estimated to be less than 0.5°C. The temperature profile measured by the Sabreliner instrumentation within the cloud boundary was randomly perturbed assuming a normal distribution with a 0.5°C standard deviation and the resulting profiles of ϵ_{cld} and K retrieved for ten model runs. The resulting K values were within +/- 3% and the mean absolute error in the cloud emittance was about +/- 0.005.

The assumed profile of water vapor influences the retrieval of ϵ_{cld} and K because the model separates the emission due to water vapor from that due to the cloud ice water. If, for example, the amount of water vapor is overestimated, then ϵ_{cld} will be underestimated. The measured water vapor profile shown in Fig. 2.2 was randomly perturbed and 10 test profiles were generated assuming an error in water vapor mixing ratio as large as 100%. The resulting K values were within +/- 18% and the values of ϵ_{cld} within +/- 0.03. It is estimated that the actual uncertainty in the water vapor measurements is about +/- 10%. For this case, a +/- 10% uncertainty in water vapor mixing ratio produced K values within +/- 3% and a mean absolute error in cloud emittance of about +/- 0.003.

2.2.4 The Effect of Errors in Cloud Top Height Estimates

Cloud top heights were estimated from visual analyses of the videotapes recorded in flight. Although it was sometimes difficult to ascertain the presence or absence of clouds overhead (i.e. 19 October), the cloud top heights estimated for the cloud layers described

here should be accurate to +/- 2 *mb*. In order to examine the effect of errors in cloud top height estimates on the retrieval of ϵ_{cld} and K, the model was run for the 31 October case with the cloud top height specified to be 5 *mb* lower than the original estimate. The irradiance at this level was obtained by linear interpolation between the measurements at 10.9 *km* and 10.3 *km*. The resulting errors in ϵ_{cld} and K were most extreme in the upper layer of the cloud where the error in K was about 6% and the error in ϵ_{cld} was nearly 25%. For the other two layers, the errors in K were 0.5% and 0.07%, respectively while the errors in ϵ_{cld} were 4% and 1%, respectively. These results indicate the high sensitivity of the ϵ_{cld} in the top layer to this thickness change while the total emittance for the entire cloud remains nearly the same. In addition, K is relatively insensitive to this thickness change implying its utility in representing the relationship between the microphysical and radiative properties of cirrus clouds.

2.2.5 Summary of Error Analyses

Table 2.2 summarizes the results of the error analyses described above. These results give the maximum error for the entire cloud and are comparable to the expected precision of the available data. Furthermore, these errors are similar but slightly better than those reported by Griffith, *et al.*, (1980). One final test was performed in which all of the parameters in Table 2.2 were allowed to vary simultaneously in a random manner. This test was performed 600 times to test the effect of simultaneous measurement errors on the retrieval of ϵ_{cld} and K. 90% of the emittance values were found to be within +/- 0.09. The range in the retrieved K values was much larger due to the high degree of uncertainty in the ice water content. 90% of the K values were found to be within 56% of the desired value.

Table 2.2: Summary of Error Analyses

Parameter	Expected Precision of Data	Resulting Errors	
		Emittance	K
Irradiance (Random Errors)	$2\ Wm^{-2}$	+/- 0.01	+/- 9%
Irradiance (Bias Errors)	$5\ Wm^{-2}$	+/- 0.02	+/- 8%
Ice Water Content	50%	0.0	+/- 50%
Temperature	0.5°C	+/- 0.005	+/- 3%
Water Vapor Mixing Ratio	10%	+/- 0.003	+/- 3%
Cloud Top Height	5 mb	+/- 0.02	+/- 2%
Maximum Cumulative Error (90% Confidence Limits)		+/- 0.09	+/- 56%

2.3 Horizontal Variability - Definitions

The horizontal variability in the broadband, infrared and shortwave properties of the cirrus cloud systems investigated here are characterized in terms of several radiation parameters. These parameters are defined as the broadband infrared (4–50μm) downward effective emittance ($\epsilon^* \downarrow$), the upward effective emittance ($\epsilon^* \uparrow$), the shortwave (.3–2.8μm) effective extinction (ς) and the shortwave albedo (ρ) by the following equations.

$$\epsilon^* \downarrow = \frac{H_B^{IR} \downarrow - \overline{H}_T^{IR} \downarrow}{\sigma \overline{T}_B^4 - \overline{H}_T^{IR} \downarrow} \tag{9}$$

$$\epsilon^* \uparrow = \frac{H_T^{IR} \uparrow - \overline{H}_B^{IR} \uparrow}{\sigma \overline{T}_T^4 - \overline{H}_B^{IR} \uparrow} \tag{10}$$

$$\varsigma = \frac{\overline{H}_T^{SW} \downarrow - H_B^{SW} \downarrow}{\overline{H}_T^{SW} \downarrow} \tag{11}$$

$$\rho = \frac{H_T^{SW} \uparrow - \overline{H}_B^{SW} \uparrow}{H_T^{SW} \downarrow} \tag{12}$$

In this set of equations, $\overline{T}_T$ and $\overline{T}_B$ are the cloud top and base temperatures, the superscripts SW and IR signify shortwave or infrared irradiance (H) with the subscripts T and B indicating incidence at the cloud top or base. These equations restrict the variability

in $\epsilon^* \downarrow$ and ς to be dependent only on the downwelling irradiance values ($H_B^{IR} \downarrow, H_B^{SW} \downarrow$) at cloud base, the variability in $\epsilon^* \uparrow$ to be dependent only on the upwelling irradiance values ($H_T^{IR} \uparrow$) at cloud top and the variability in ρ to be dependent on the upwelling and downwelling irradiance ($H_T^{SW} \uparrow, H_T^{SW} \downarrow$) at cloud top. It is noted that there may be a significant reflected component of the upwelling irradiance inherent in $\epsilon^* \downarrow$ and ς. It should also be pointed out that since the effective emittance (ϵ^*) is defined as the ratio between the observed change in irradiance versus that change which would occur if the cloud were a blackbody, $\epsilon^* \downarrow$ and $\epsilon^* \uparrow$ are defined here as functions of the cloud base and cloud top temperatures, respectively. This definition implies that if a cloud were black, it would radiate at some temperature near or at its boundary (i.e. T_T or T_B). The choice of which temperature to use in the calculation of ϵ^* is really a matter of definition and should depend on where the effective radiating temperature of the cloud is located within the cloud boundaries. This really depends on the mass distribution within the cloud (Abakumova, *et al.,* 1980). For cirrus clouds, most of the mass (IWC) is concentrated in the lower half of the cloud as is evident in Figs. A.3, A.5, A.7, and A.9 in Appendix A. For the calculation of the downwelling irradiance, the most significant contribution comes from the lower part of the cloud where the emittance increment is the largest and so the effective radiating temperature will likely be located near the cloud base. However, for the calculation of the upwelling irradiance, the emittance increment is largest near the middle of the cloud since most of the mass is concentrated in the lower portion. This implies that the effective radiating temperature in the upwelling direction will likely be poorly approximated by the cloud top temperature and better approximated by the mid-cloud temperature. In this study, we have chosen to adhere to the conventional definitions of effective emittance as defined by Eqns. 9 and 10.

Chapter 3

RESULTS

The analysis of the five cirrus layers described here was divided into three parts. First, the data were analyzed to infer cloud emittances (ϵ_{cld}) and broadband, infrared absorption coefficients (K) to deduce the impact of the layers on infrared radiation. The relationship of the absorption coefficients to temperature and microphysical characteristics of the clouds are explored. Because only one aircraft was used, measurements at different levels in the cloud were not made simultaneously. As a result, sampling errors may occur due to the nonsteady state of the cloud field and/or due to the possibility that the flight legs were not flown directly above or below each other. To minimize these errors and in an attempt to set some limits on the observed radiative properties (ϵ_{cld} and K), the downwelling irradiance and IWC data for each flight leg were averaged in the following ways:

MEAN: Average using every measurement along the flight leg to determine a mean value for the cirrus cloud field.

THINNER: Average the lowest 30% of the irradiance measurements and the lowest 30% of the IWC data to represent the optically thinner part of the cloud field.

THICKER: Same as above but for the highest 30% to represent the optically thicker part of the cloud field.

Second, the horizontal variability in the BBIR and BBSW radiative properties of the cirrus systems are investigated and compared. Finally, current methods of parameterizing the radiative properties of cirrus are discussed and assessed in comparison to the new data presented here.

3.1 Radiative Properties

3.1.1 Cloud Emittance

The model deduced cloud emittances, that is, the emittances due solely to the cloud ice water, are shown as a function of ice water path (IWP) in Fig. 3.1 for the five cirrus clouds for the case using the flight leg means. For the geometrically thinner clouds (19 Oct., 28 Oct.), the emittance approaches about 0.4-0.5 while for the geometrically thicker clouds (22 Oct., 31 Oct.) the emittance approaches 0.7-0.8. This figure indicates that ϵ_{cld} is a similar function of IWP for the five cirrus clouds sampled during FIRE. It is interesting to note that if one were to fit the data points in Fig. 3.1 with a single regression line, the model deduced values of ϵ_{cld} would lie well within the +/- 0.09 margin of error (see Table 2.2) determined in Section 2.2.4. Also depicted in Fig. 3.1 is the emittance-IWP relationship deduced by Griffith *et al.,* (1980) for a tropical cirrus case observed during GATE. In their study, they reported observations of anvil cirrus close to deep convection. This relationship is considerably different from that deduced from the FIRE data. There are a number of possible reasons for this discrepancy. The first is that the discrepancy is real, resulting from some fundamental difference between the radiative properties of the midlatitude and tropical 'anvil' types of cirrus. The second is that Griffith *et al.,* (1980) may have underestimated the ice water contents inferred from the 1-dimensional particle imaging probes flown during GATE. Such an underestimate (assuming that the estimates from the FIRE data are correct) need be of considerable magnitude to explain the discrepancy in Fig. 3.1 but the possibility does exist. The third and most likely explanation concerns an apparent bias in the irradiance measurements that were reported by Griffith and Cox (1977) from which the emittance-IWP relationships of Griffith *et al.,* (1980) were deduced. Griffith and Cox (1977) noted, without explanation, that there were problems with the absolute measurement of irradiance since the measured downwelling flux often exceeded the blackbody flux in the cirrus clouds sampled during GATE. In addition, they measured downwelling irradiance values above cloud top (at a height near 12 km) on the order of 80 Wm^{-2}. These measurements exceed the broadband infrared radiative transfer and LOWTRAN-7 calculations of clear sky flux (in a standard tropical

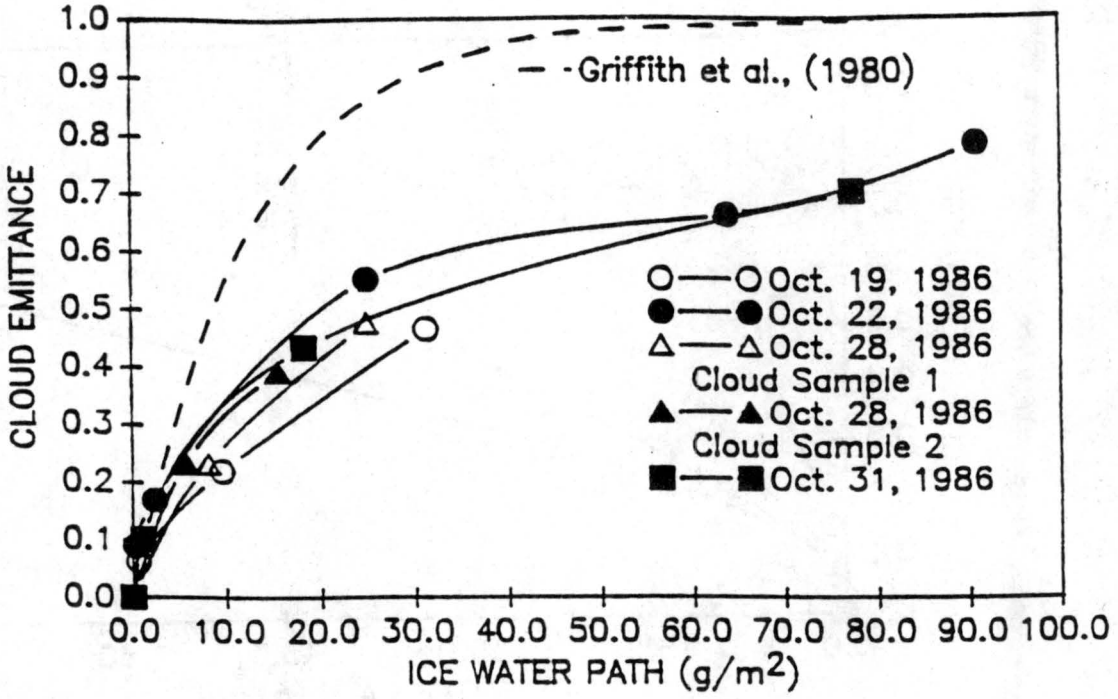

Figure 3.1: Model deduced cloud emittance (ϵ_{cld}) for five cirrus cloud systems sampled during FIRE, as a function of ice water path (IWP). The dashed line is taken from the data of Griffith *et al.*, (1980).

atmosphere at the same altitude) by over 50 Wm^{-2}. It is possible that the presence of a cirrus deck above 12 km could account for this difference, however such occurrences were not reported. It is more likely that calibration or instrument error produced biases in the irradiance measurements during GATE. This could lead to overestimates in cirrus cloud emittances. For example, if one computes the effective emittance (ϵ^*, defined in Section 2.3) for two irradiance profiles of similar slope but offset from one another, the profile with the higher irradiance values will yield a higher effective emittance. This argument may be extended to the cloud emittance (ϵ_{cld}) since ϵ_{cld} and ϵ^* are linearly related (see Fig. 2.9). Therefore, it is suggested here that the emittance values reported in Griffith and Cox (1977) and Griffith *et al.*, (1980) were overestimated due to biases in the absolute measurement of irradiance. Furthermore, the magnitude of these overestimates is similar to the magnitude of the discrepancy shown in Fig. 3.1.

Figs. 3.4-3.7 depict the resulting cloud emittances for the stratified irradiance and IWC profiles described in Section 4.0. Once again, the primary motivation for stratifying the data in this way was an attempt to minimize the possibility of sampling errors and to

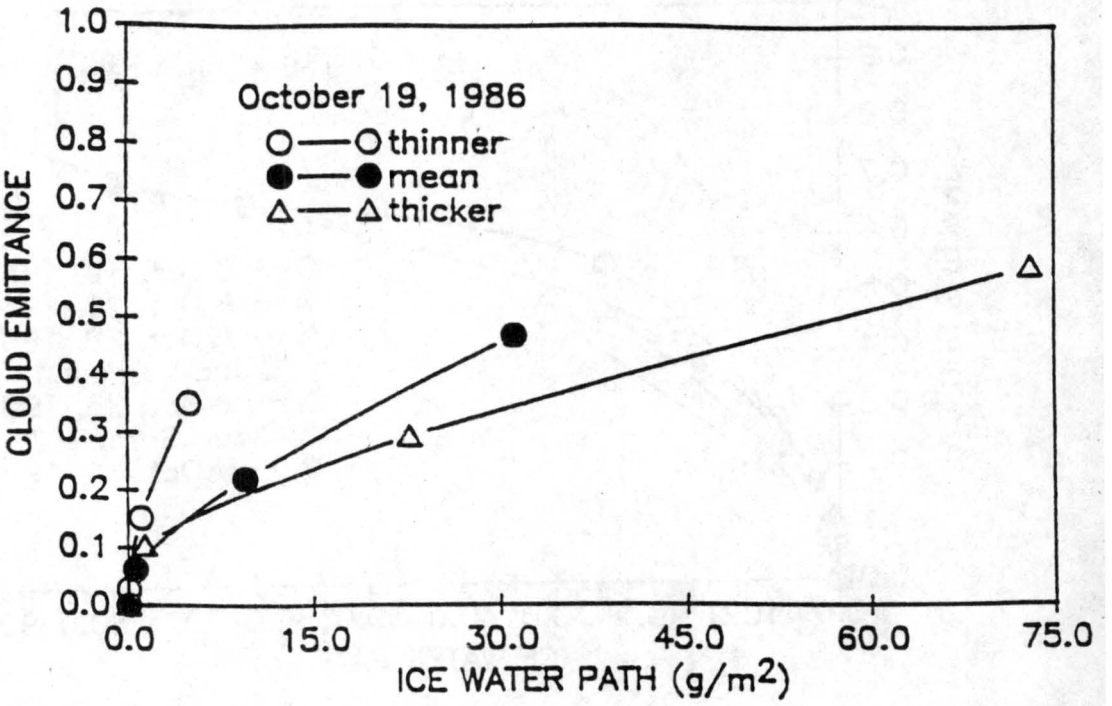

Figure 3.2: Model deduced cloud emittance (ϵ_{cld}) as a function of ice water path (IWP) for the stratified data of October 19.

set some limits on the observed radiative and microphysical properties since the vertica and horizontal structure of these cirrus clouds are both complicated and highly variable For the case of 19 October, ϵ_{cld} was about 0.35 for the thinner cloud and 0.60 for the thicker cloud. Narrower ranges in ϵ_{cld} were found for the other cases and particularly for 22 October where the emittance values for the mean and thicker clouds exhibit a simila functional dependence on IWP. The thinner cloud case on 22 October was excluded from Fig. 3.5 because the resulting irradiance profile through one of the layers was apparently "more clear" than the profile calculated for the clear sky. It is interesting to note that in every case except 19 October, the functional dependencies of the cloud emittance on IWP are similar between the mean and thicker cloud, but not for the thinner clouds It is possible that when stratifying the data as described above, the infrared radiativ properties of the thinner clouds are being significantly modulated by unmeasured sma particles.

Stackhouse and Stephens (1989) have shown that small particles (d< 50μm) ca significantly modulate the transfer of infrared radiation. Furthermore, Prabhakara, *et al* (1988) and Ackerman, *et al.*, (1989) have demonstrated that a unique spectral signatur

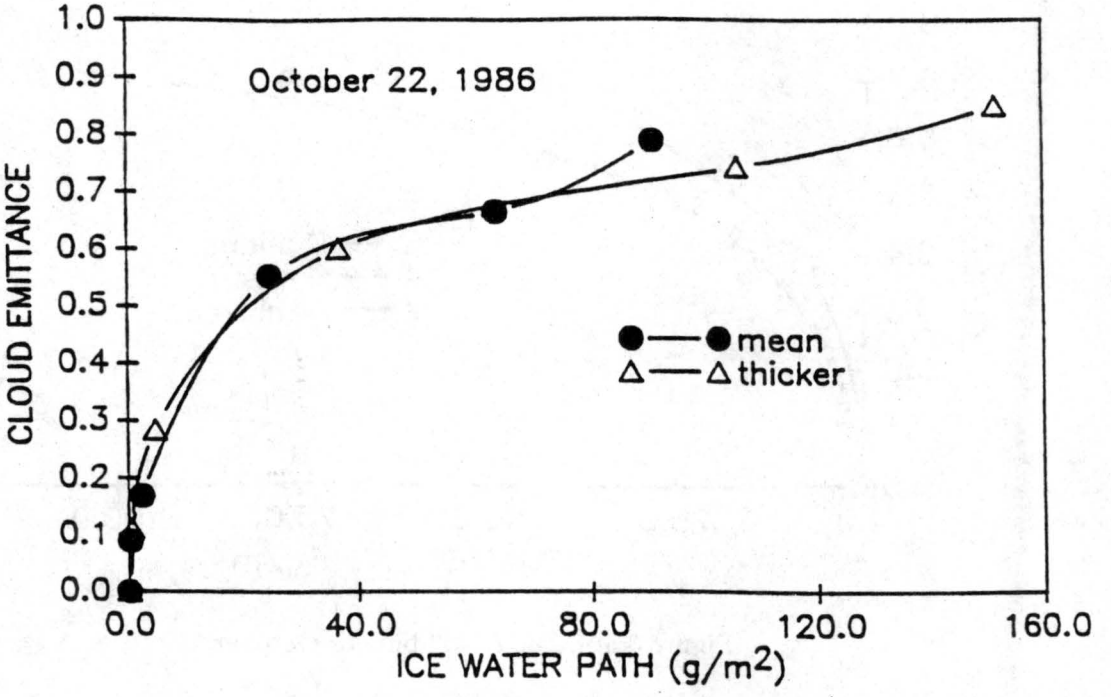

Figure 3.3: Same as 3.2 but for October 22.

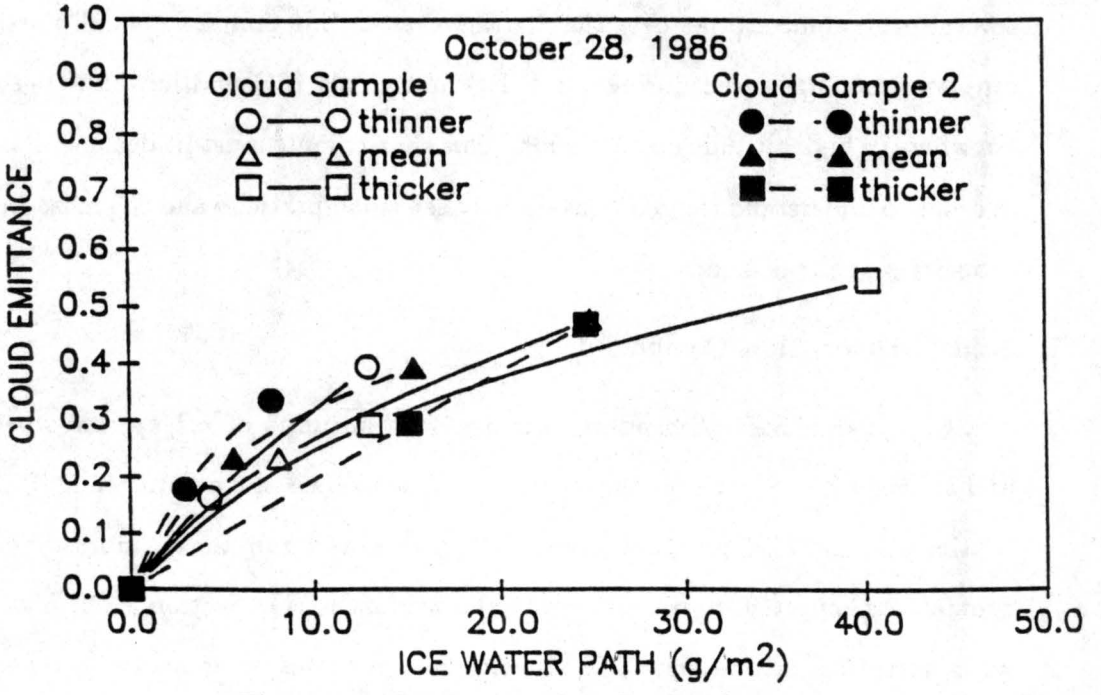

Figure 3.4: Same as 3.2 but for October 28.

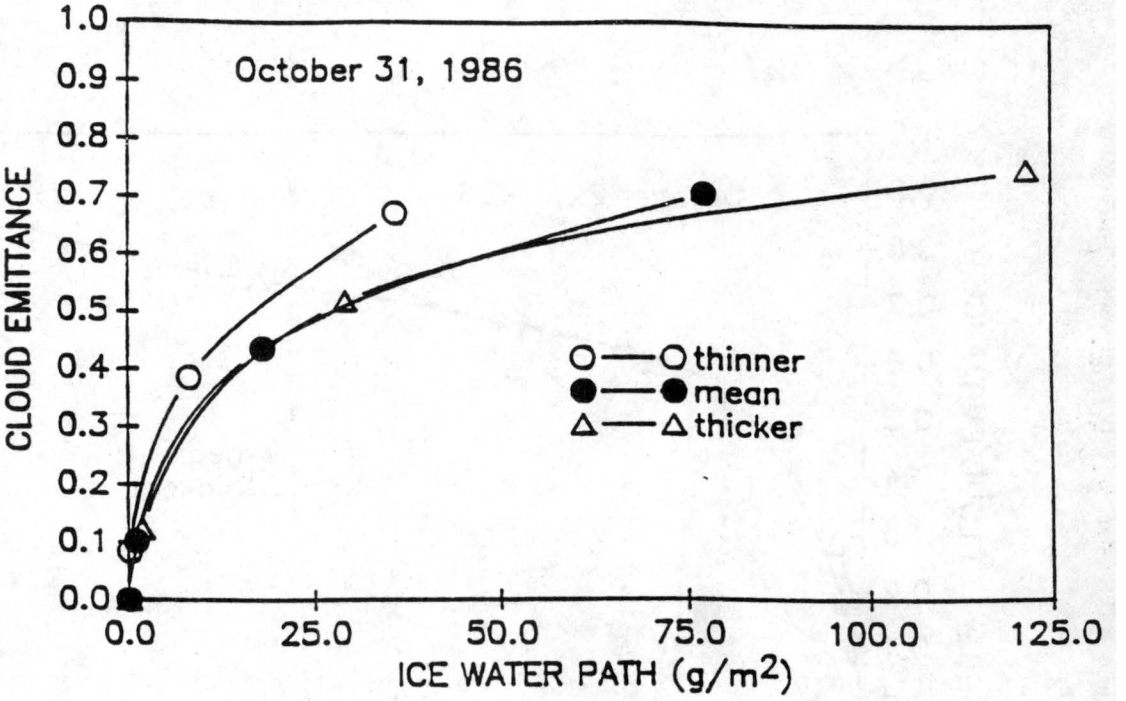

Figure 3.5: Same as 3.2 but for October 31.

which occurs across the infrared window region (8-12 μm) due to cirrus clouds is consistent with radiative transfer calculations for ice particle size distributions with effective radii less than 40 μm. Marwitz (1987) reported measurements of small particle size distributions in several orographic storms over the Sierra Nevada. Unfortunately, small particles (d<36 um) were not measured during the FIRE first cirrus IFO and have not been measured anywhere in high altitude cirrus clouds. This shortcoming must be dealt with in the future in order to understand the relationship between small particles and the measured radiative properties of cirrus clouds.

3.1.2 Absorption Coefficients

Broadband mass absorption coefficients (K in units of m^2/kg) have been deduced and are shown in Fig 3.8 for the five cirrus clouds versus the parameter $\overline{D}_{mass}$ (defined in Section 2.1.2). This figure shows the K values retrieved from the mean irradiance and IWC profiles. As expected from the theoretical considerations in Section 2.1.2, K does decrease with increasing particle size. The magnitude of K varies by about two orders from abou 0.48 m^2g^{-1} to 0.007 m^2g^{-1}. Table 3.1 summarizes the mass absorption coefficients c

Table 3.1: Compilation of mass absorption coefficients deduced for cirrus clouds.

$K(m^2/g)$	Source
0.056	Paltridge & Platt, 1981;broadband flux emittance
0.051	Paltridge & Platt, 1981;effective beam emittance(11μm)
0.076-0.096	Griffith et al., 1980;broadband flux emittance in tropical cirrus
0.007-0.48	This study

cirrus deduced by several other authors. Griffith *et al.*, (1980) deduced K values of 0.096, 0.080 and 0.076 m^2g^{-1} to fit irradiance observations of three cirrus clouds observed during a tropical eastern Atlantic experiment (GATE). Paltridge and Platt (1981) deduced a K value of 0.056 m^2g^{-1} to fit irradiance observations of cirrus cloud decks over New Mexico. This investigation is the first which attempts to deduce profiles of K through cirrus clouds. The physical significance of K as it is defined in Eqns. 3 and 4 may best be described as a coefficient which relates the IWP to all other microphysical characteristics important to the modulation of the incident irradiance. These other microphysical characteristics probably include, but may be not limited to, the effects of small particles, particle orientation and ice crystal habit. The functional dependence of K on the parameter $\overline{D}_{mass}$ shown in Fig. 3.8 appears to be somewhat dissimilar from one cirrus cloud to the next although the general negative slope is common to all cases. This may indicate that the microphysical properties that the K values characterize in Eqn. 3 are dissimilar from one cirrus cloud to the next. Figs. 3.9-3.12 depict the retrieved K values for each cirrus case for the different cloud stratifications. As in the case of the cloud emittance and particularly for 19 October and 31 October, the functional dependence of K for the mean and thicker stratifications are similar to each other but rather different from that of the thinner clouds. Because small particles were not measured, it is possible that IWC has been underestimated. The underestimate in IWC is expected to be less than 15% (Heymsfield and Miller, 1989). A test was performed to determine if the high values of K deduced for the thinner clouds may be the result of IWC underestimates due to the exclusion of the unmeasured smaller particles. It was determined that the IWC values need be an unrealistic 2-5 times larger for the thinner clouds in order to retrieve K values similar to those retrieved for the

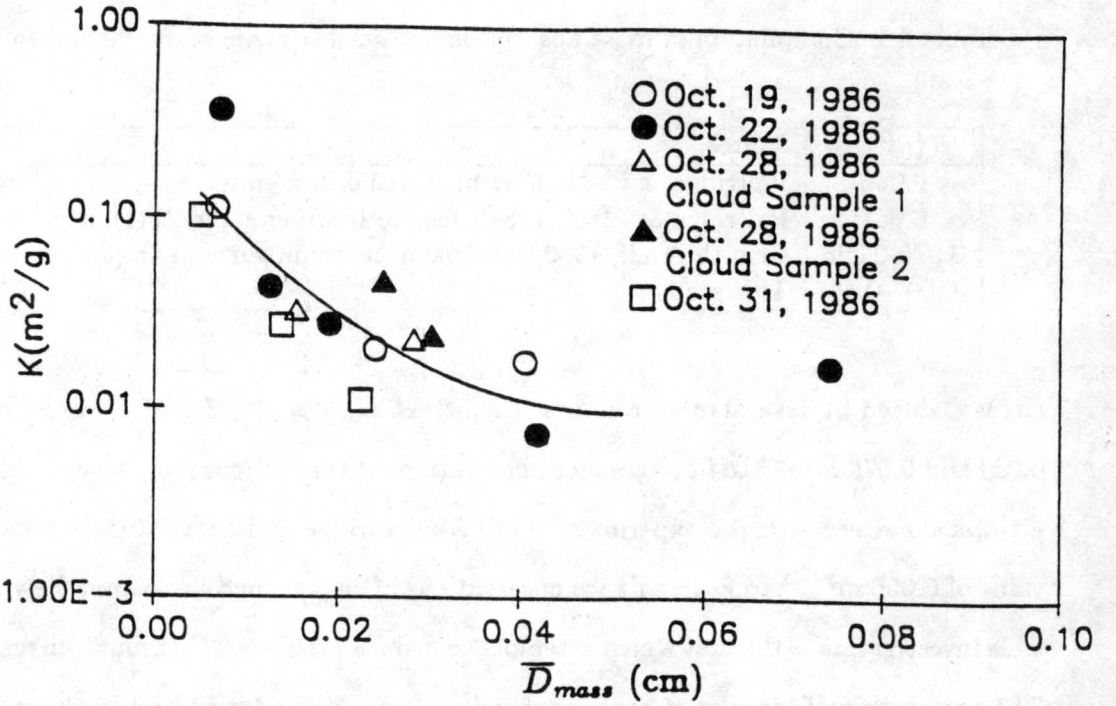

Figure 3.6: Mass absorption coefficients (K) as a function of the parameter $\overline{D}_{mass}$ for five cirrus cloud systems.

mean case. Similarly, errors in the cloud thickness (ΔZ) estimates need be on the order of several kilometers, considerably larger than the expected error. It is possible that the radiation data stratified into the thinner clouds are more effectively characterized by smaller particles. In other words, the thinner clouds represent data with lower IWC and lower irradiances, however the high values of K that are retrieved from this data may indicate the significant effect of some unmeasured microphysical characteristic. This could be attributed to small particles by considering the theoretical arguments in Section 2.1.2 which suggest that K is inversely proportional to particle size. It is noted that K is also proportional to the absorption efficiency (Q_a), which decreases with a decreasing size parameter ($\frac{2\pi r}{\lambda}$). Thus, for wavelengths in the infrared, a decrease in the particle size will result in a decrease in Q_a but at a slower rate which implies via Eqn. 5 that for cirrus clouds, the large K values obtained in the thinner clouds may indicate the presence of small particles.

Platt and Harshvardhan (1988) (hereafter referred to as PH) discuss the temperature dependence of cirrus infrared extinction based on data obtained by Platt, *et al.*, (1987

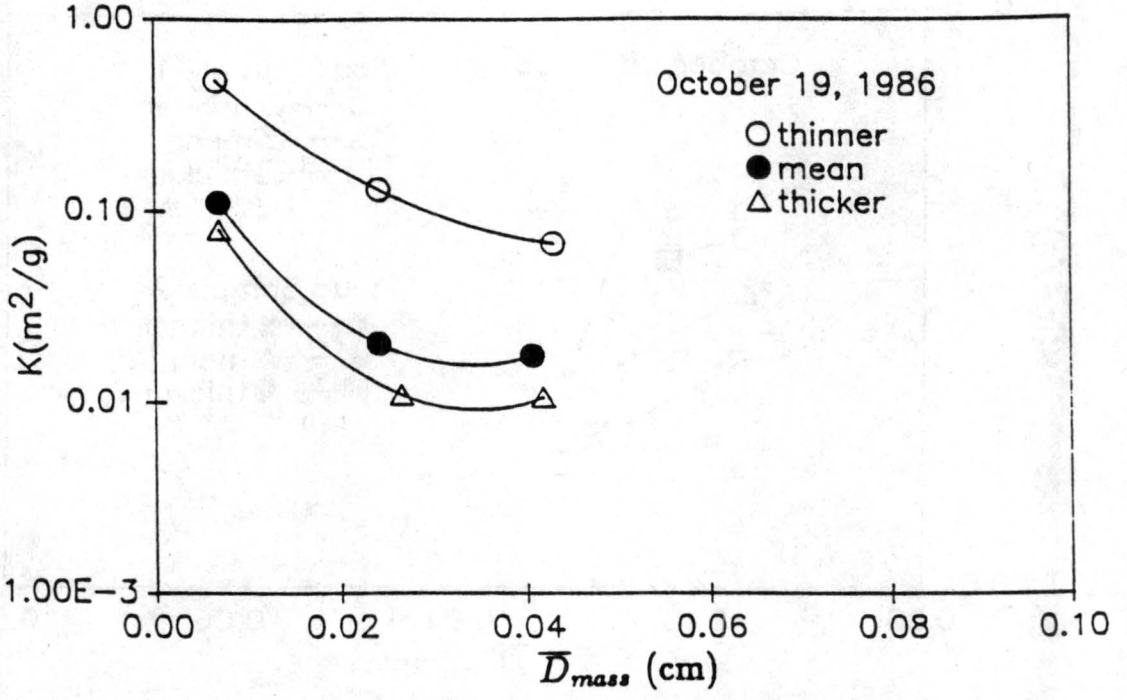

Figure 3.7: Mass absorption coefficients (K) as a function of the parameter $\overline{D}_{mass}$ for the stratified data of October 19.

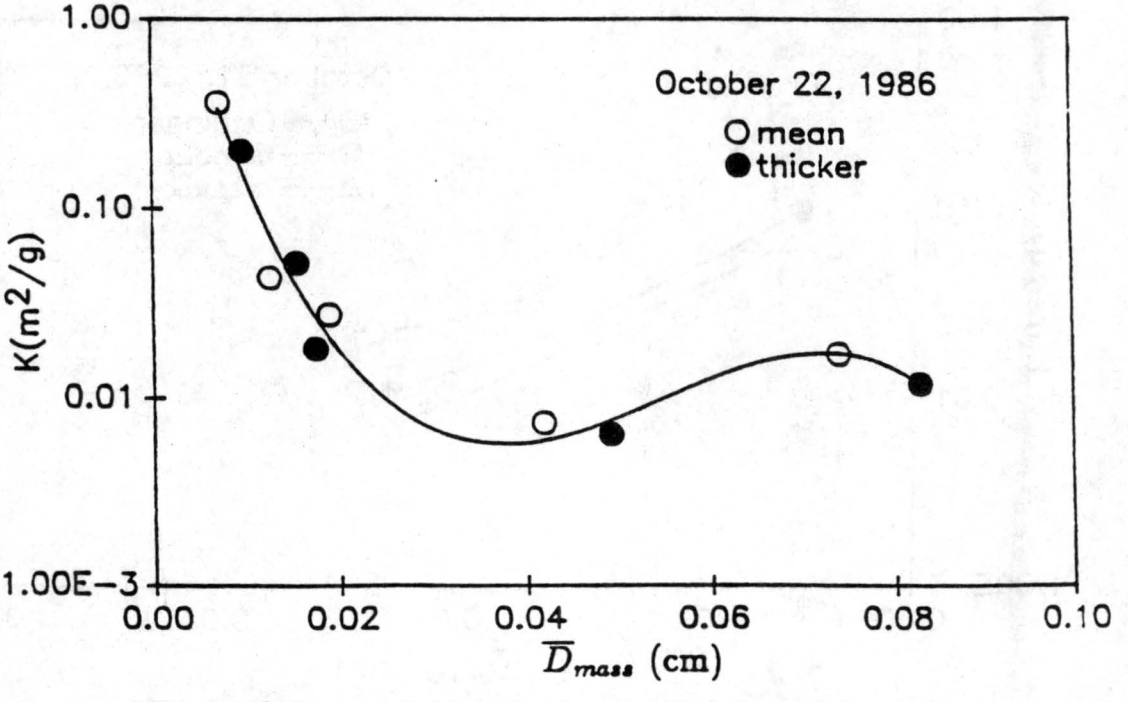

Figure 3.8: Same as 3.7 but for the stratified data of October 22.

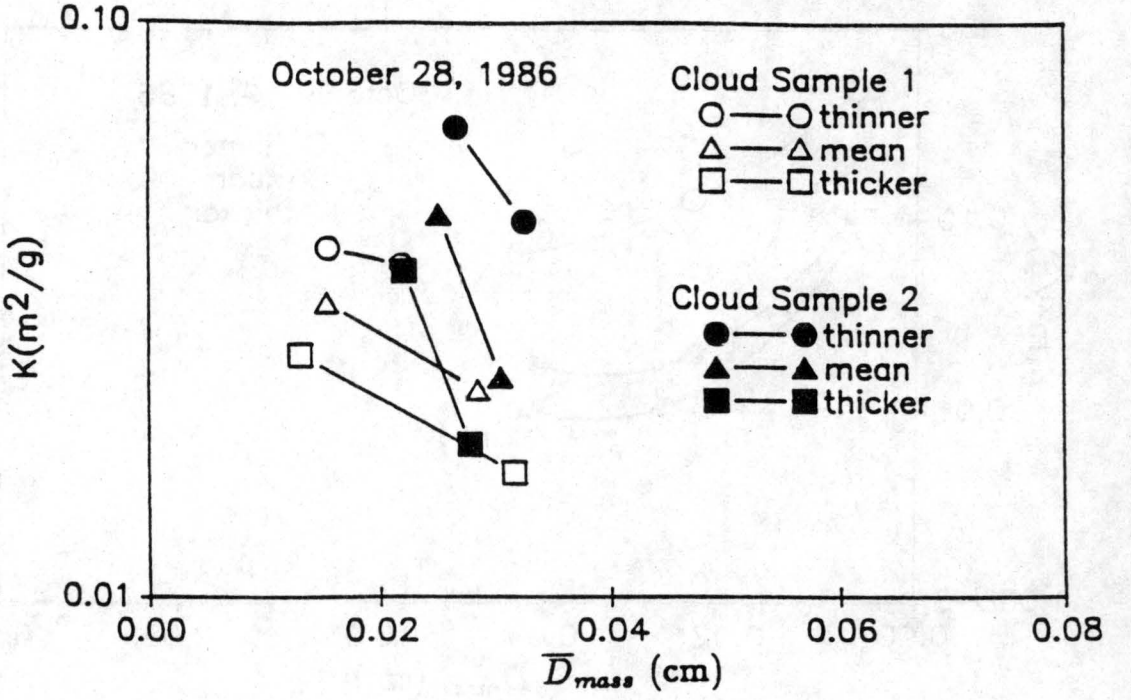

Figure 3.9: Same as 3.7 but for the stratified data of October 28.

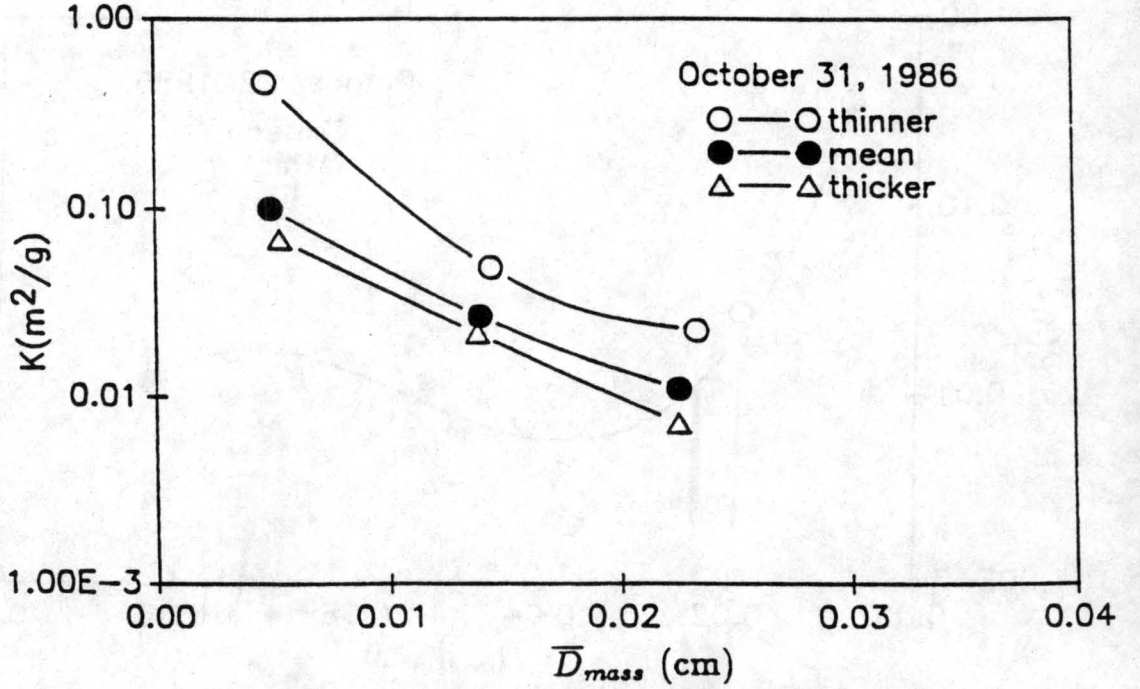

Figure 3.10: Same as 3.7 but for the stratified data of October 31.

and Heymsfield and Platt (1984). The beam absorption coefficients (10-12 μm) deduced from these two independent data sets were found to be similar functions of temperature. Broadband absorption coefficients (σ) have been computed where

$$\sigma = K \cdot IWC \tag{13}$$

for the five cirrus clouds examined here and for the mean, thinner and thicker cloud cases. σ for the mean cloud case is plotted as a function of temperature in Fig. 3.13 against two regression lines for the data in PH. The solid line fits the beam absorption coefficients as presented in PH while the dashed line fits these same values multiplied by a diffusivity factor of 1.66. Figs. 3.14 and 3.15 show a similar comparison but for the stratified data of 28 October and 31 October. The agreement between the σ values calculated in this study and the regression lines from PH is very good. It should be noted that the data of PH were obtained by first deducing a single absorption coefficient from ground-based radiometer and lidar observations of a cirrus cloud with some mid-cloud temperature. The absorption coefficients were then averaged for many clouds with similar mid-cloud temperatures. Here, absorption coefficients have been determined as a function of depth through cirrus clouds and have been related to the mean temperature of the appropriate layer. The degree with which these two data sets compare may suggest that the bulk infrared properties of cirrus may be parameterized as a function of temperature.

3.1.3 Horizontal Variability

Frequency distributions of $\epsilon^* \uparrow$, $\epsilon^* \downarrow$ and ς are shown in Figs. 3.16-3.27 for the five cirrus cloud cases. On 19 October, $\epsilon^* \uparrow$ varied from about 0.2 to 0.5 (Fig. 3.16). $\epsilon^* \downarrow$ was observed to vary from 0.4 to 0.7 (Fig. 3.20) while the values of ς were relatively small (Fig. 3.24), ranging from near 0.0 to about 0.3 In this case, there is some evidence that some of the values of $\epsilon^* \uparrow$ were underestimated due to the presence of low level clouds during the flight leg near cloud base which were not present during the flight leg near cloud top.

On 22 October, $\epsilon^* \uparrow$ varied from about 0.8 to 0.9 (Fig. 3.17), as would be expected for a cloud of this thickness. The values of $\epsilon^* \downarrow$ shown in Fig. 3.21 ranged from 0.7 to 0.8 while ς (Fig. 3.25) varied from about 0.45 to 0.55.

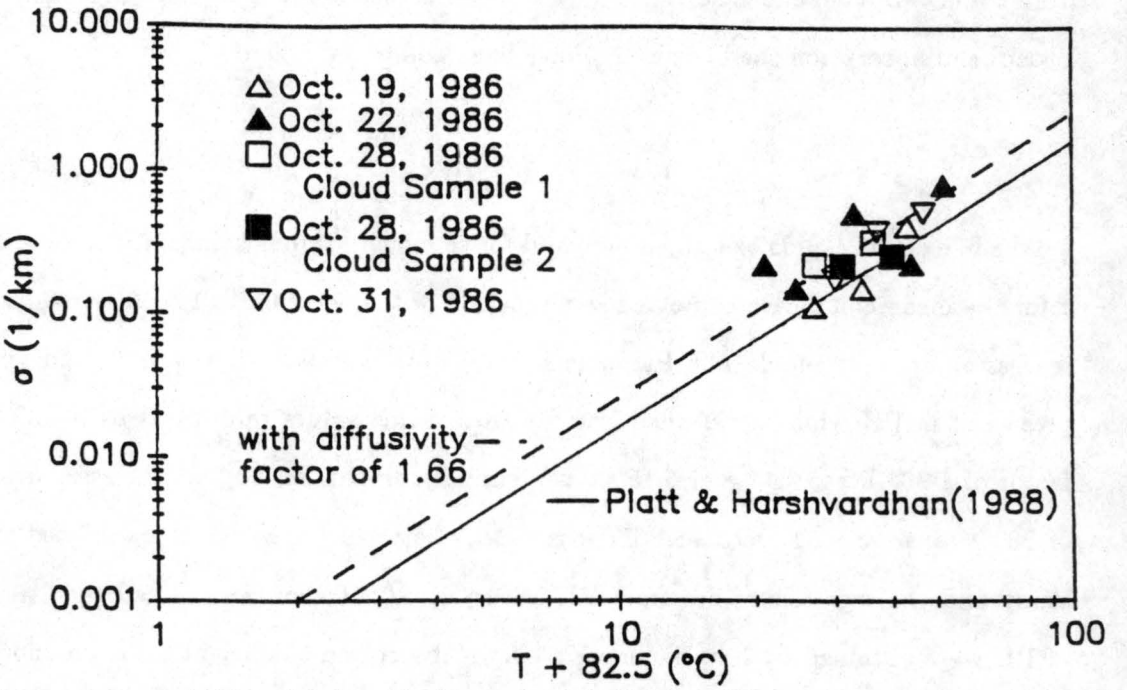

Figure 3.11: Broadband infrared absorption coefficients (σ) as a function of temperature for five cirrus clouds. The dashed line is from the data of Platt and Harshvardhan (solid line) multiplied by a diffusivity factor of 1.66

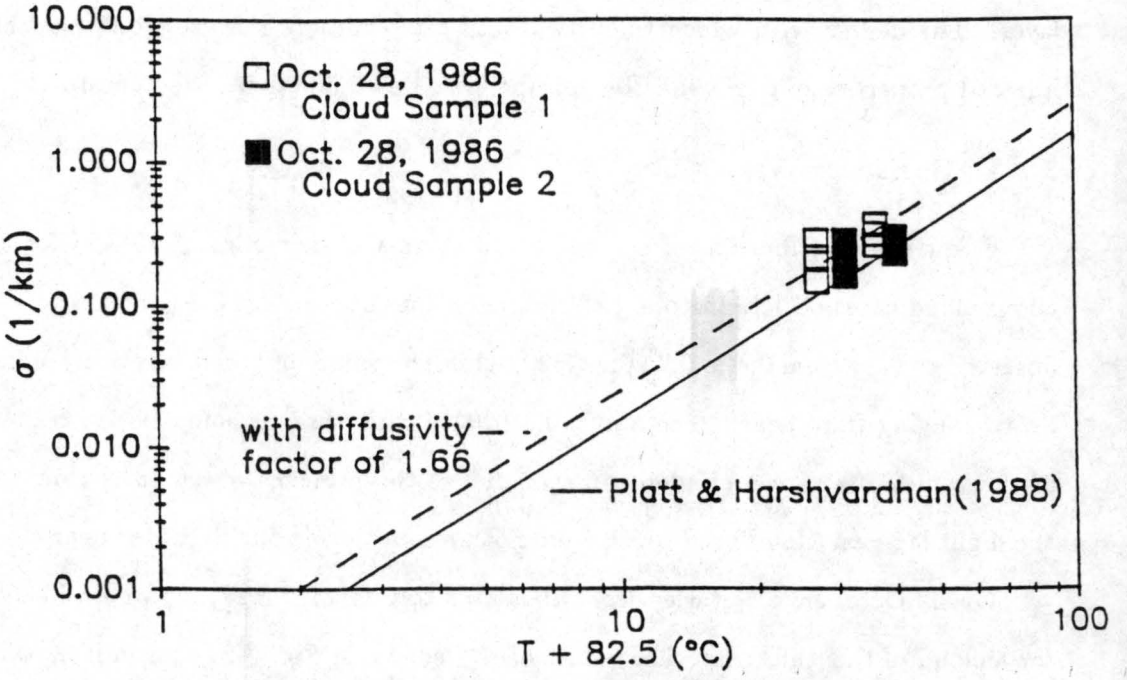

Figure 3.12: Same as 3.11 but for the stratified data of October 28.

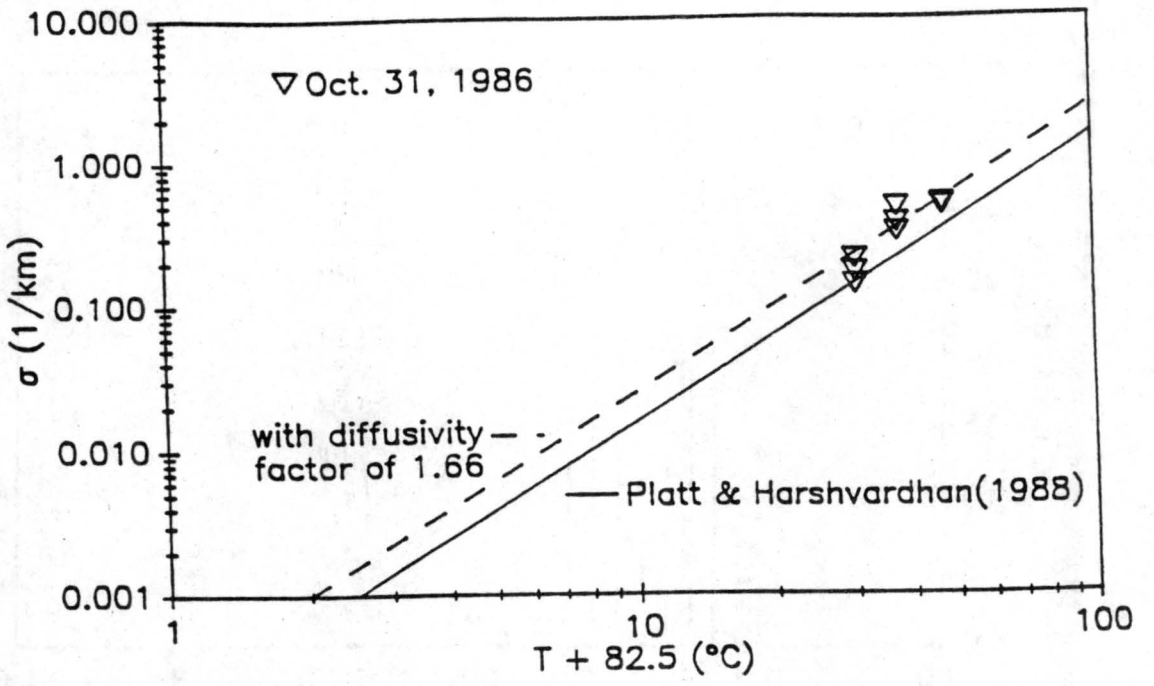

Figure 3.13: Same as 3.11 but for the stratified data of October 31.

On 28 October, $\epsilon^* \uparrow$ ranges from about 0.35 to 0.6 (Fig. 3.18). These values have been shown to be similar to those deduced from satellite observations (Stephens, *et al.*, 1989). A similar range in $\epsilon^* \downarrow$ is shown in Fig. 3.22. On this day, ς ranged from near 0.05 to about 0.32 (Fig 3.26). These data have been described in Smith Jr., *et al.*, (1989) where differences in the radiative properties of the two clouds sampled were attributed mainly to differences in the clouds geometric thickness.

On 31 October, the range in $\epsilon^* \uparrow$ was from 0.25 to 0.4 (Fig. 3.19) whereas the range in $\epsilon^* \downarrow$ was from about 0.65 to 0.72 (Fig. 3.23) and the range in ς was from 0.3 to 0.35 (Fig. 3.27). It appears that the $\epsilon^* \uparrow$ values have been underestimated for similar reasons as those given above for 19 October. In this case, it's probable that the radiative properties of the low level undercast were not constant throughout the Sabreliner flight. The profile of mean upwelling irradiance appeared rather jagged and in fact, the mean irradiance at one level was on more than one occasion very similar to the mean irradiance at a level below. This analysis seems to indicate that the upwelling infrared irradiances measured near the cloud base may have been significantly lower than the upwelling irradiances which occurred at

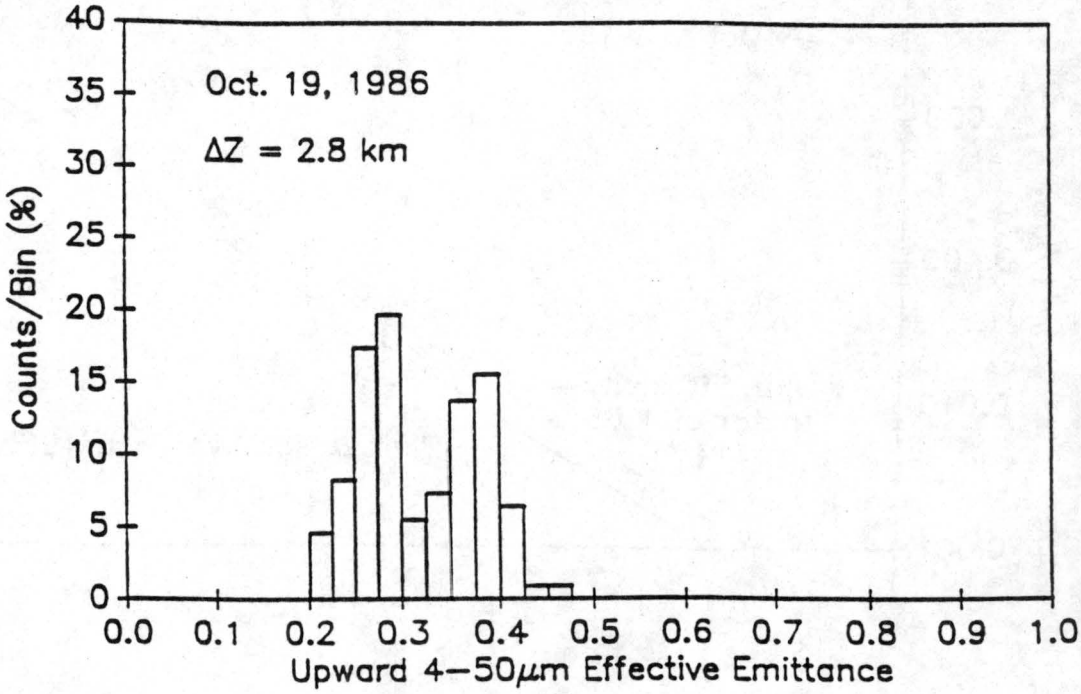

Figure 3.14: Frequency distribution of the upward effective emittance for a cirrus cloud sampled on October 19, 1986.

the cloud base when the Sabreliner sampled data at the cirrus cloud top. Therefore, it's possible that all of the $\epsilon^* \uparrow$ values have been underestimated.

There are several similarities in the frequency distributions described above that warrant some discussion. First, the range in the broadband infrared (BBIR) radiative properties, characterized by $\epsilon^* \downarrow$, and the range in the broadband shortwave (BBSW) radiative properties, characterized by ς are very similar within each case. This suggests that the BBIR and BBSW radiative properties of cirrus may be well correlated. Fig. 3.28 supports this and illustrates the degree of correlation for all five cirrus clouds in a plot of ρ versus $\epsilon^* \uparrow$. ς and $\epsilon^* \downarrow$ were found to be less correlated and there was considerable scatter due to cloud heterogeneities since the downwelling shortwave irradiance was considerably more variable than the downwelling infrared irradiance. With the exception of 31 October, the data plotted in Fig. 3.28 also support the conclusion of Stephens, *et al.*, (1989) that the characterization of cirrus microphysical properties from Mie theory (which generally yields an asymmetry parameter (g) of about 0.87) will be unrealistic unless the asymmetry parameter is forced to be some value closer to 0.7. Stephens, *et al.*, (1989) also showed that

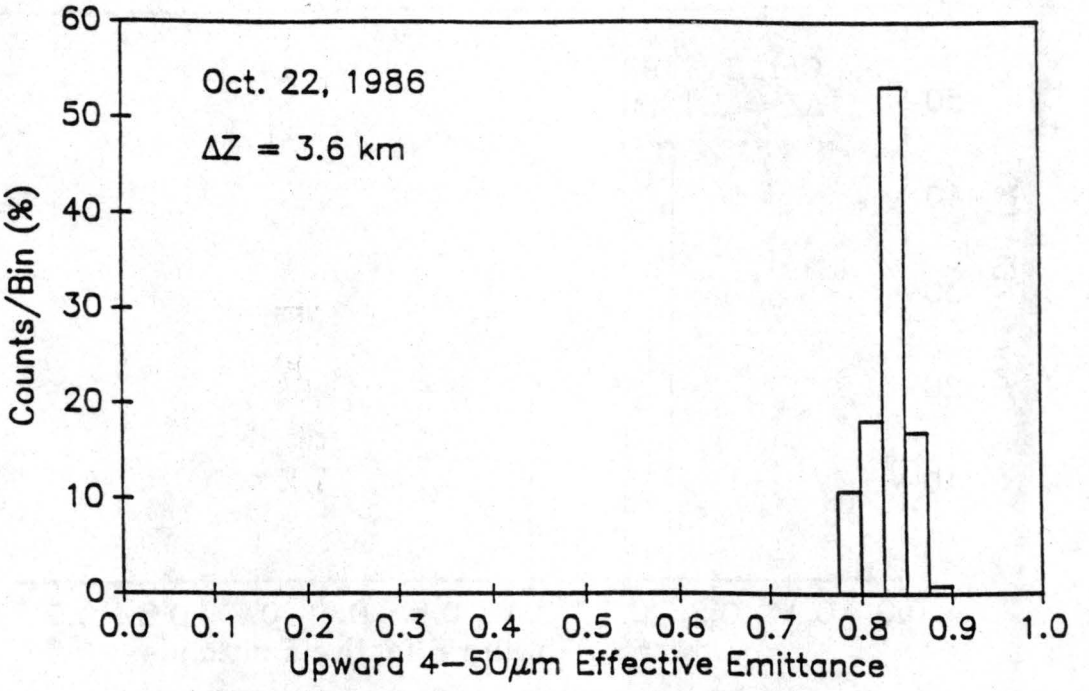

Figure 3.15: Same as 3.14 but for October 22, 1986.

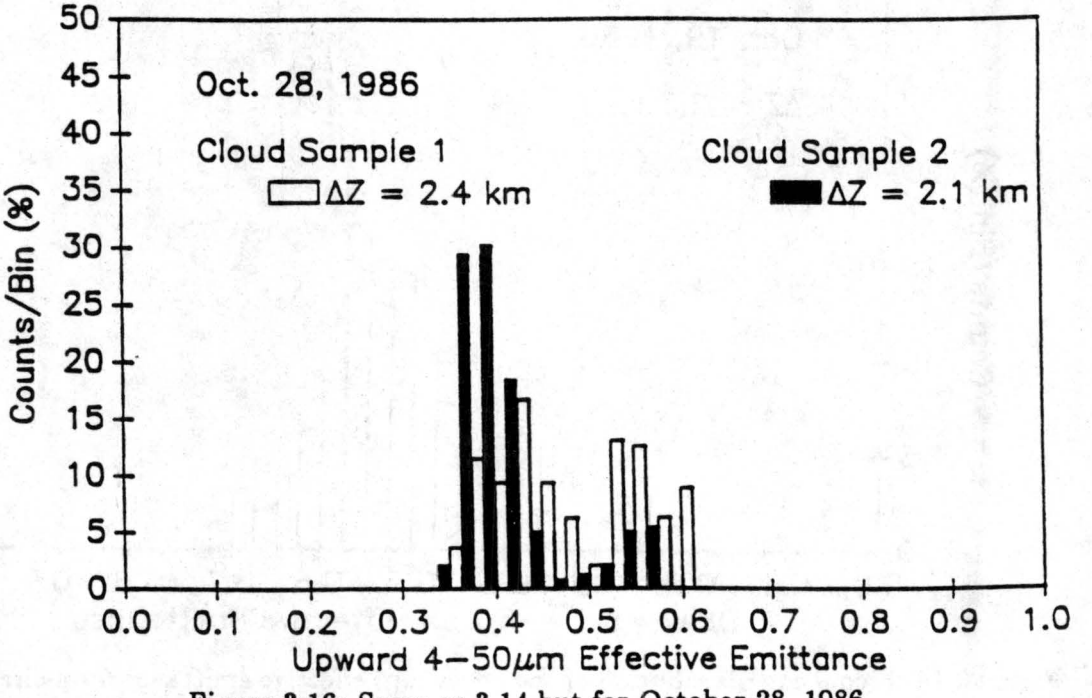

Figure 3.16: Same as 3.14 but for October 28, 1986.

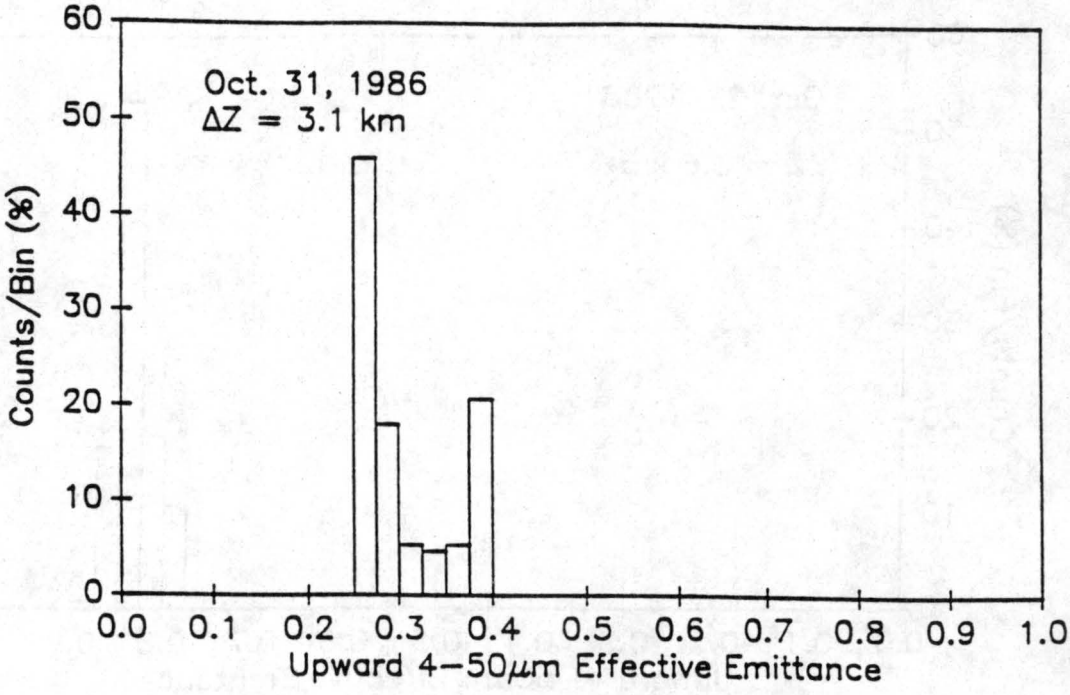

Figure 3.17: Same as 3.14 but for October 31, 1986.

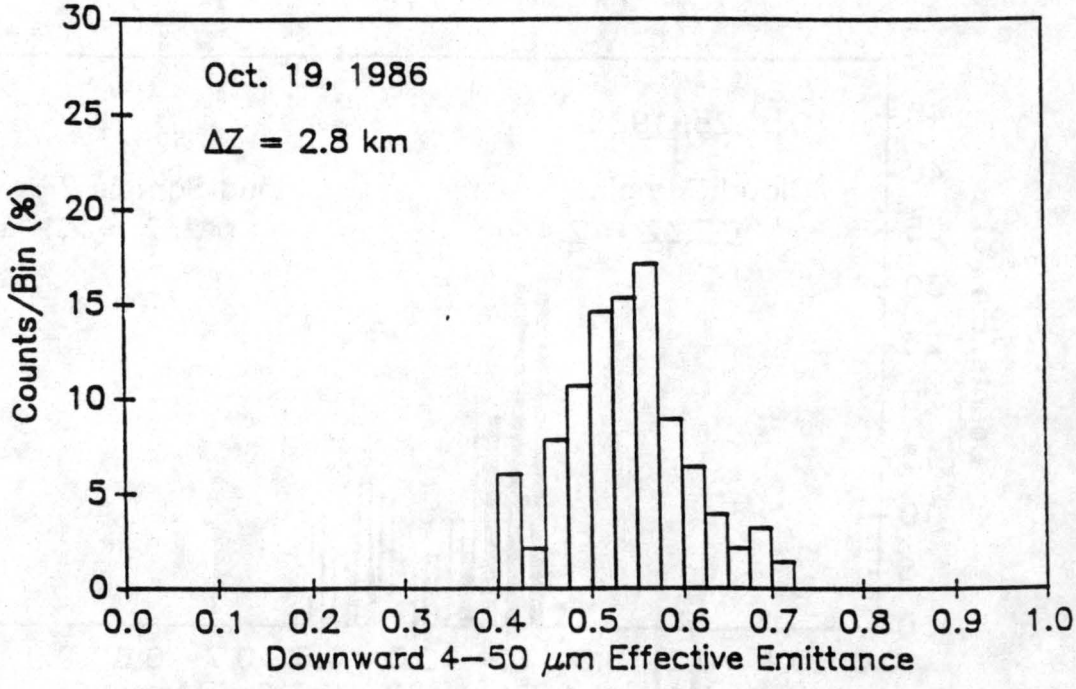

Figure 3.18: Frequency distribution of the downward effective emittance for a cirrus cloud sampled on October 19, 1986.

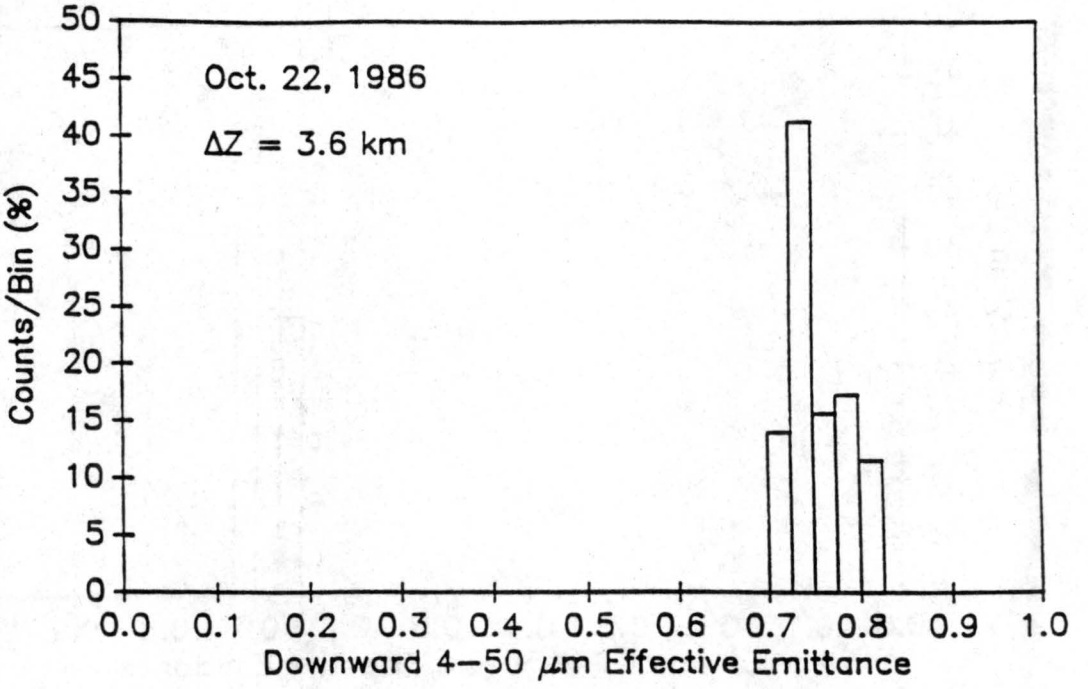

Figure 3.19: Same as 3.18 but for October 22, 1986.

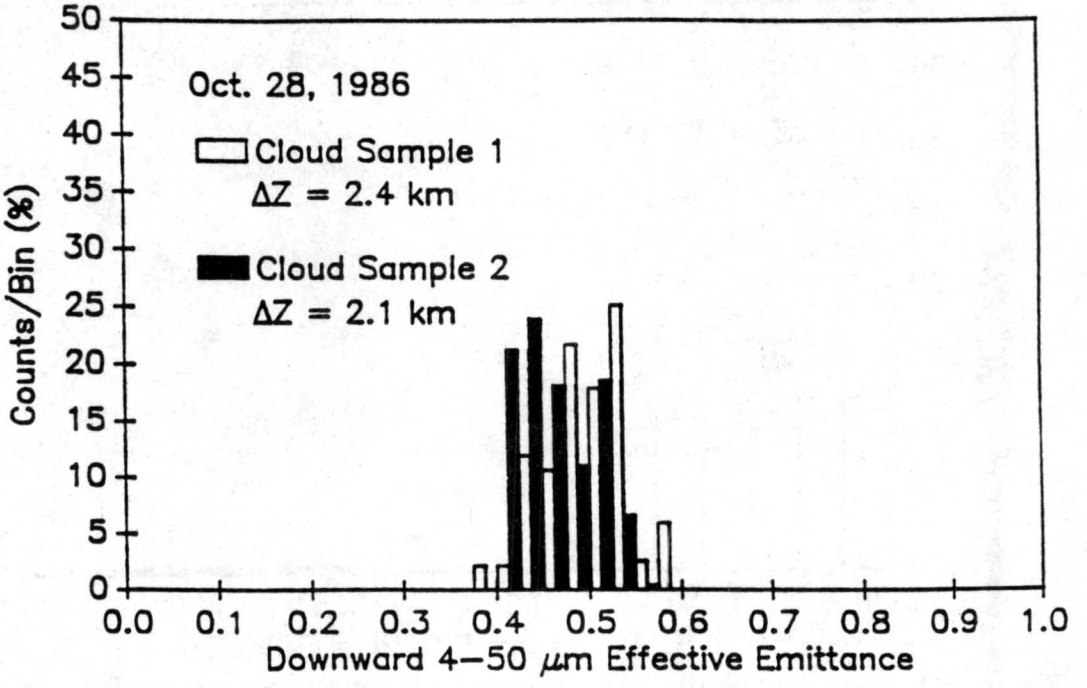

Figure 3.20: Same as 3.18 but for October 28, 1986.

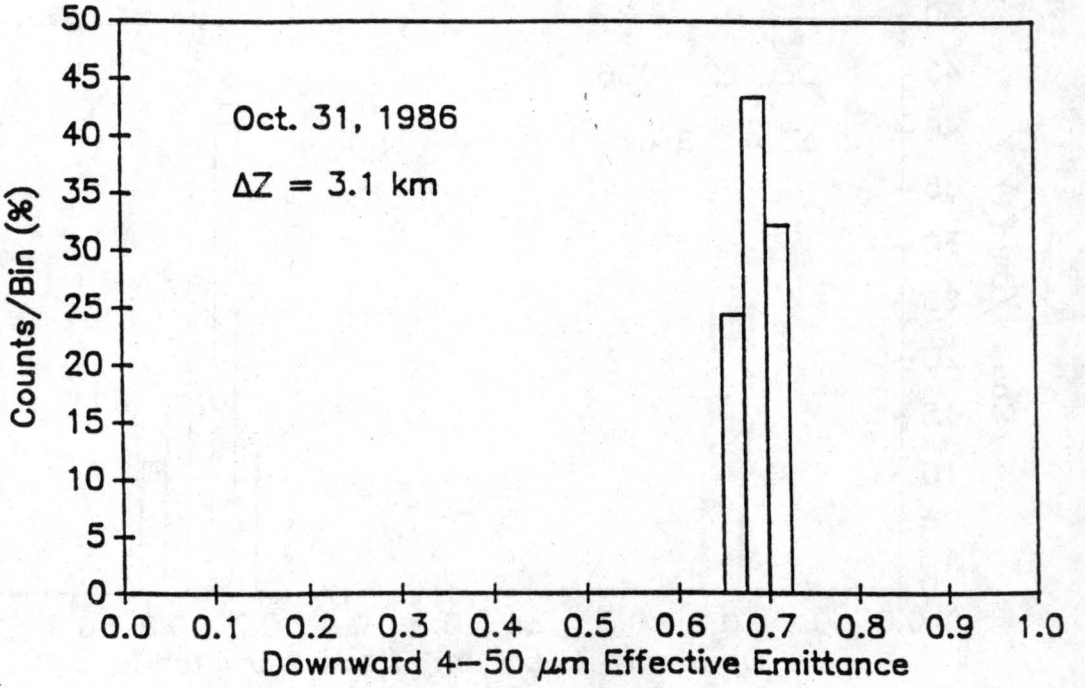

Figure 3.21: Same as 3.18 but for October 31, 1986.

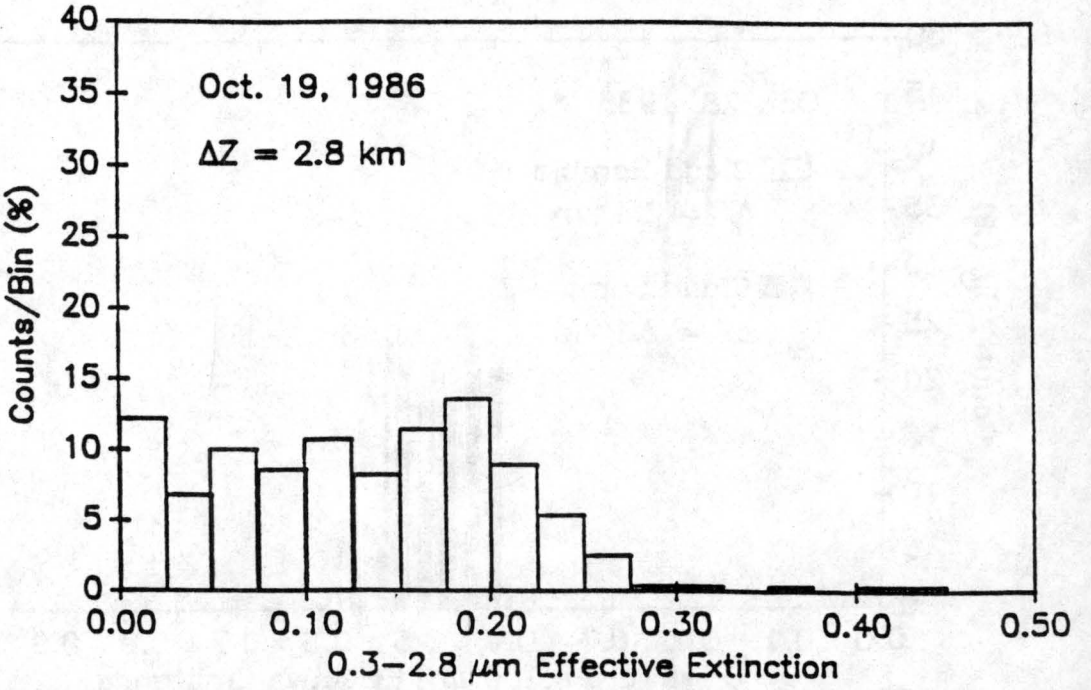

Figure 3.22: Frequency distribution of the shortwave effective extinction for a cirrus cloud sampled on October 19, 1986.

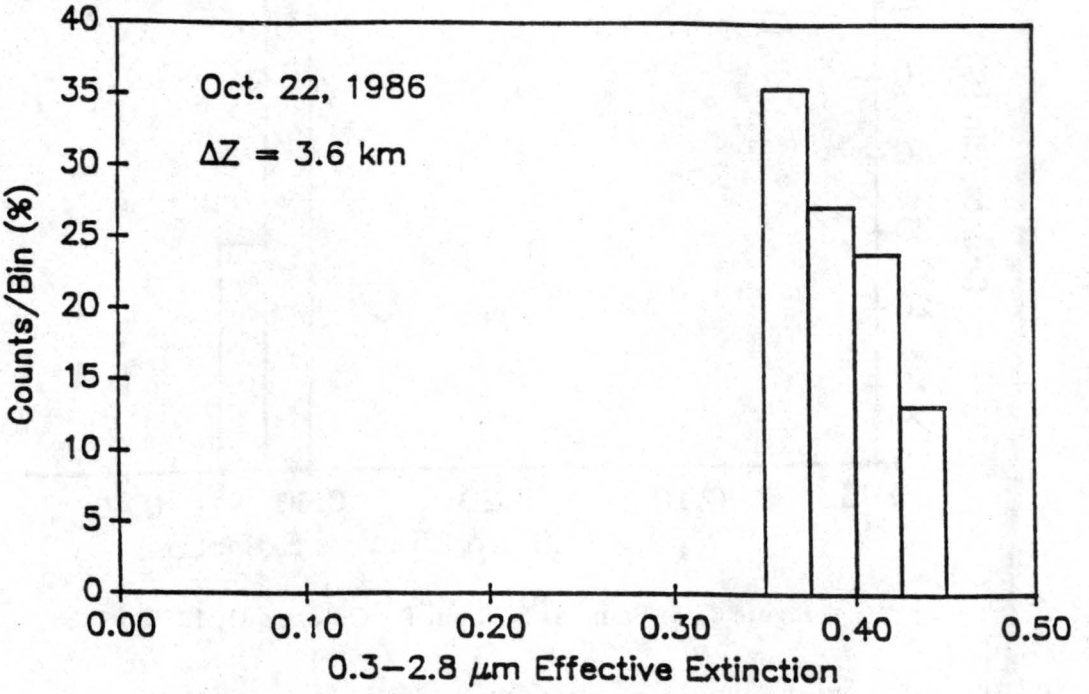

Figure 3.23: Same as 3.22 but for October 22, 1986.

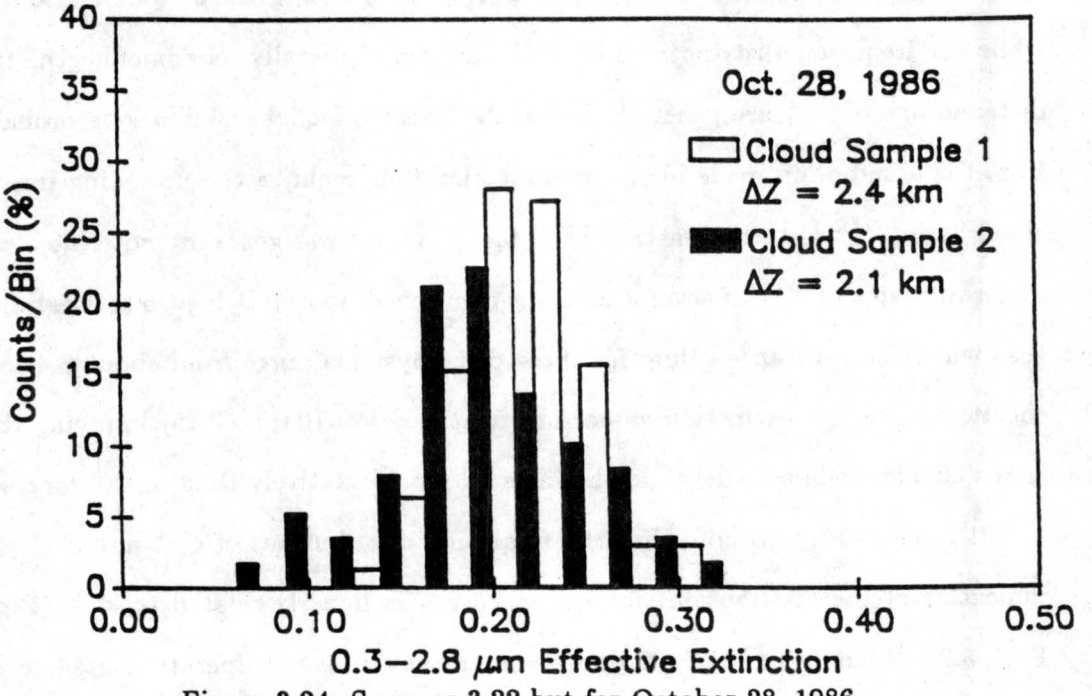

Figure 3.24: Same as 3.22 but for October 28, 1986.

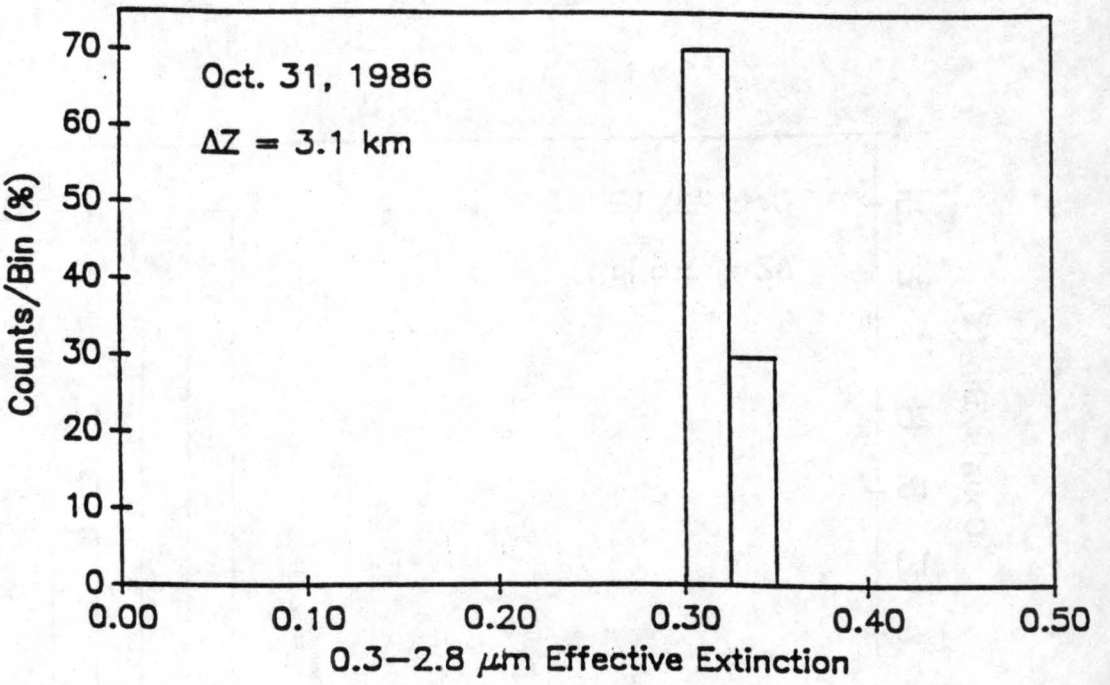

Figure 3.25: Same as 3.22 but for October 31, 1986.

the theoretical albedo-emittance relationships in Fig. 3.28 showed no appreciable change from those obtained assuming different effective radii (r_e). The high albedos deduced from the data of 31 October are likely the result of the very high zenith angle (75°). The zenith angles for the other three flights were around 60°. Figs. 3.16-3.27 also show that while the frequency distributions for $\epsilon^* \downarrow$ and ς are generally monomodal, the frequency distributions of $\epsilon^* \uparrow$ are generally bimodal. These bimodal distributions probably arise from the assumption made in the computation that requires the upwelling irradiance at cloud base ($H_B^{IR} \uparrow$) to be constant. The fact that this was generally not true also lead to underestimates of $\epsilon^* \uparrow$ in several cases as mentioned above. It is also interesting to note that while the emittance values for these cloud systems range from about 0.4 to 0.8, the shortwave effective extinction values are relatively low (0.0 to 0.45) implying that these cirrus clouds modulate energy in the infrared more effectively than in the shortwave.

It is interesting to note that the frequency distributions of $\epsilon^* \uparrow$ and $\epsilon^* \downarrow$ should be indicative of the distributions for ϵ_{cld} since ϵ_{cld} is linearly related to $\epsilon^* \downarrow$ (Fig. 3.29). Fig. 3.29 differs from Fig. 2.9 due to differences in the temperature used to compute the effective emittance ($\epsilon^* \downarrow$) as discussed in Section 2.3. In Fig. 2.9, $\epsilon^* \downarrow$ is always

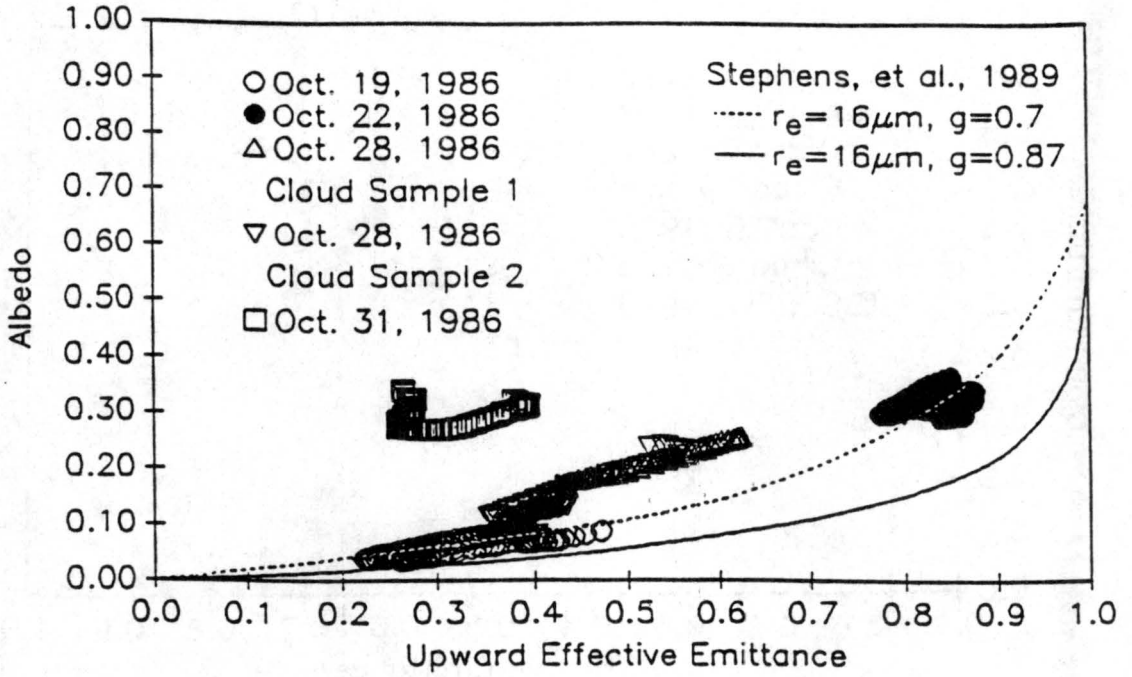

Figure 3.26: Albedo versus the upward effective emittance deduced from aircraft observations of five cirrus clouds. The solid (dashed) line represents the theoretical curve developed by Stephens, *et al.*, 1980 using an asymmetry parameter of 0.87 (0.7).

greater than ϵ_{cld}, which is what one may expect since $\epsilon^* \downarrow$ includes the emission due to the atmospheres gases. In Fig. 3.29, $\epsilon^* \downarrow$ is less than ϵ_{cld} for emittances greater than about 0.6. This is due to the fact that the temperature at the base of the layer is used to compute $\epsilon^* \downarrow$ (Eqn. 9) while the determination of ϵ_{cld} results from a more representative radiative transfer calculation which considers the multi-layered contribution of temperature to the downwelling irradiance using the average temperature of the layers (Eqn. 2.2). Therefore, the effective radiating temperature of the cloud is lower for the case of ϵ_{cld} so that ϵ_{cld} is greater than $\epsilon^* \downarrow$. Note that both $\epsilon^* \downarrow$ and ϵ_{cld} inherently contain the effects of reflected upwelling irradiance. Also, Fig. 3.28 illustrates the dominant effect of the cloud aerosol on the emittance since the contribution by the atmospheric gases is only about 0.09.

3.2 Current Methods of Parameterizing the Bulk Radiative Properties of Cirrus Clouds

Presently, one of the most challenging areas of research in the Atmospheric Sciences is in the study of global climate. Recent evidence suggests that certain human activities

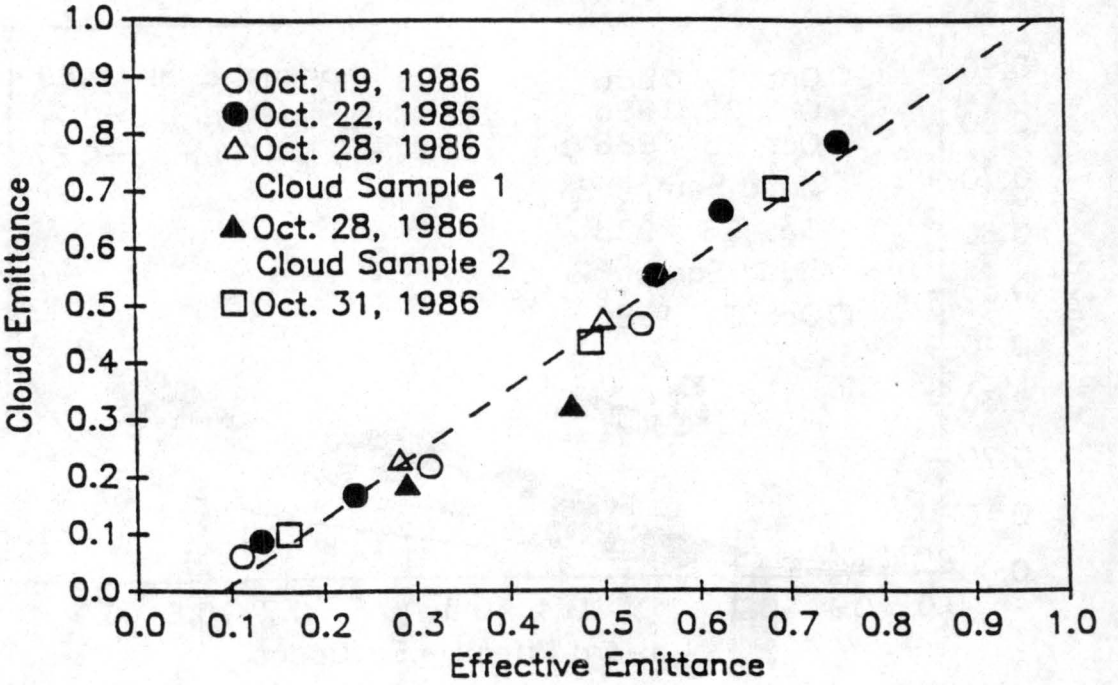

Figure 3.27: Model deduced cloud emittance (ϵ_{cld}) versus the observed effective emittance ($\epsilon^* \downarrow$) for five cirrus clouds. Here, ($\epsilon^* \downarrow$) was computed using the temperature at the base of the layer.

may alter the climate of the Earth (i.e. CO_2 and PFC emissions). Consequently, there has been a surge of interest in the study of climate and climate change. The radiative effects of cirrus clouds are known to be critical to the accuracy with which a GCM can simulate and/or predict the Earth's climate (Cox, 1971, Ramanathan, *et al.*, 1983, Wetherald and Manabe, 1988, Randall, *et al.*, 1989). This implies that an adequate representation of the radiative effects of cirrus is critical to the degree with which we may use GCM's to understand the important forcings and feedbacks of our climate. Stephens (1984) reviewed the cloud parameterization schemes employed in an assortment of numerical models. For the broadband infrared region, these schemes ranged from very crude, where all clouds are assumed to be black ($\epsilon_{cld} = 1$) to a more complex emissivity formulation similar to the one given in Eqns. 3 and 4 but assuming a constant mass absorption coefficient (K) based on the data of Griffith, *et al.*, (1980) and Paltridge and Platt (1981). The latter parameterization assumes that the infrared radiative properties of clouds are directly related to IWP, using a constant mass absorption coefficient, which clearly is not the case for cirrus clouds based on the data presented above and on the recent data of PH. Furthermore,

because the current state of cloud parameterizations in climate models is crude, it would be beneficial to develop radiation parameterizations based on some well known parameter such as temperature rather than ice water content. Such a parameterization for cirrus clouds has been introduced into the UCLA/GLA GCM (Harshvardhan, *et al.*, 1989). This parameterization is supposed to be based on the experimental data of Platt, *et al.*, (1987) and the theoretical relationship between the infrared absorption and shortwave optical depths (denoted here as τ_{ir} and τ_{sw}). PH discuss the relationship between τ_{ir} and τ_{sw} and show that for cirrus clouds, if the size parameter is large,

$$\tau_{ir} = 0.5 \cdot \tau_{sw}. \tag{14}$$

This relationship arises because the absorption efficiency (Q_a) approaches 1 in the infrared while the extinction efficiency (Q_{ext}) approaches 2 in the shortwave for large values of the Mie size parameter. Eqn. 14 has also been verified by the experimental data reported by Abakumova, *et al.*, (1980). The infrared properties of cirrus are parameterized in terms of the flux emittance (ϵ_{cld}) as defined in Eqn. 3 where $\tau_{cld} = d \cdot \tau_{ir}$ and d is the diffusivity factor. In this parameterization, τ_{ir} is not obtained from the temperature dependent relationship derived from the experimental data of Platt, *et al.*, (1989) but rather from a parameterization of τ_{sw} where

$$\tau_{sw} = b \cdot (T_c + T_o)^2 \cdot \Delta P_c. \tag{15}$$

In Eqn. 15, T_c is the mean cloud temperature, ΔP_c is the pressure thickness of the cloud and $T_o = -82.5°C$. The coefficient $b = 2.0 \cdot 10^{-6}$ was apparently obtained by trial and error using satellite-derived albedos as a guide although the exact methodology has not been ascertained. In deducing the radiative properties of clouds from in situ broadband irradiance measurements, it is generally more difficult to obtain properties in the shortwave (SW) than in the infrared since you must consider both the direct and diffuse components of the total SW flux. For example, the shortwave transmittance may be approximated as in Stephens and Tsay (1989) by

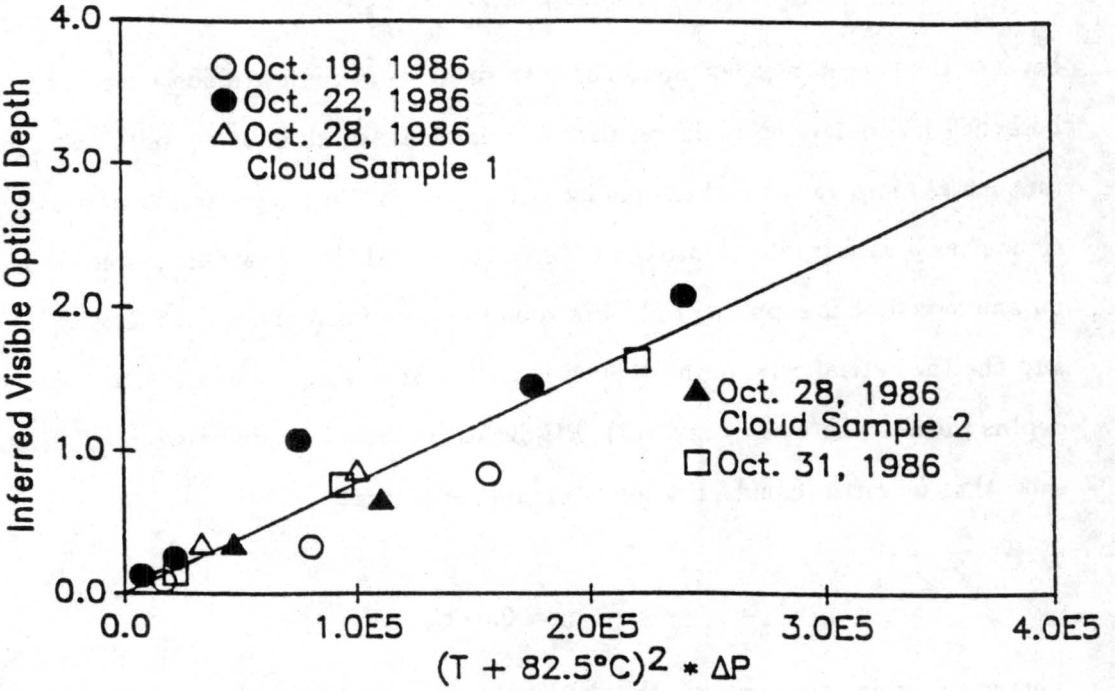

Figure 3.28: Visible optical depth (inferred from 4-50 μm optical depths deduced from the FIRE observations) as a function of temperature squared times pressure thickness.

$$\mathcal{T} = \frac{H_D \downarrow (z)}{\mu_o H_o} + exp(\frac{-\tau_{sw}}{\mu_o}), \tag{16}$$

where $H_D \downarrow (z)$ is the diffuse flux at some level z below cloud top, μ_o is the cosine of the zenith angle, $\mu_o H_o$ is the value of the flux at cloud top normal to a horizontal plane and τ_{sw} is the optical thickness of the cloud layer. Eqn. 16 implies that the determination of τ_{sw} from observations ($\mathcal{T}$ is measured) requires knowledge of either the direct or diffuse component of the total flux. Neither of these components are typically measured and were not measured from the Sabreliner during FIRE. Therefore, no attempt is made here to deduce τ_{sw} from the shortwave irradiance measurements. Instead, τ_{sw} is inferred from τ_{ir} deduced from the FIRE data using Eqn. 14 where τ_{ir} was inferred from the τ_{cld} values as defined in Eqn. 3 divided by d=1.5 in order to be consistent with the methods of Harshvardhan, *et al.*, (1989). Fig. 3.30 shows the inferred τ_{sw} as a function of temperature squared times the pressure thickness of the cloud layers.

A coefficient of $b = 7.76 \cdot 10^{-6}$ provides the best fit to these data but is nearly a factor of four times larger than the coefficient reported by Harshvardhan, *et al.*, (1989). This is

because the parameterization of τ_{sw} in Eqn. 14 has been scaled down to account for the fact that a GCM grid box is often times only partially filled with cloud. Thus, the grid box average optical depth is usually much less than the local optical depth that would be measured by an aircraft flying in the box (Harshvardhan and Randall, 1985). How accurate this scaling factor is probably is not well known and thus poses an important question regarding the representation of sub-grid scale clouds and cloud radiative properties in GCM's. In terms of finer resolution cirrus cloud models (i.e. Starr and Cox, 1985), a coefficient of $b = 7.76 \cdot 10^{-6}$ should be used in the cirrus cloud radiation parameterization outlined above since this parameterization is consistent with the in situ observations made during FIRE and with the data of Platt and Harshvardhan (1988) and Heymsfield and Platt (1984).

Chapter 4

CONCLUSIONS

The bulk radiative and microphysical properties of five cirrus clouds sampled via the NCAR Sabreliner on four days during the FIRE first cirrus IFO have been described. A broadband, infrared radiative transfer model was employed to deduce the impact of the cirrus layers on infrared radiation. This model isolates the effect of the atmospheric gases from that of the cloud ice water permitting retrieval of the cloud emittance (ϵ_{cld}) and profiles of the mass absorption coefficient (K). The model was extensively tested to determine how well it could retrieve ϵ_{cld} and (K) when the input data contained errors. The magnitude of these errors are comparable to the expected precision of the input data.

For the five cirrus cloud cases, ϵ_{cld} was found to range from about 0.4 to 0.8. The deduced emittance profiles were found to be similar functions of IWP. This relationship was considerably different from that deduced by Griffith *et al.*, (1980) for tropical cirrus observed during GATE. It is suggested that large errors in the absolute measurement of irrradiance may have lead to overestimates in ϵ_{cld} in their study. The mass absorption coefficients, K, were found to decrease with increasing particle size ranging from about 0.48 m^2g^{-1} in the top of one layer to about 0.007 m^2g^{-1} near the base of another. This relationship was dissimilar from one cirrus system to the next suggesting the significant effect of some unmeasured microphysical property. Small particles, which have been shown by other authors to be prevalent in cirrus clouds via the spectral characteristics remotely sensed in the 8-12 μm window region, are a likely suspect. Unfortunately, the nonexistence of quantitative measurements of small particles in high altitude cirrus has limited our ability to understand the complicated interaction between radiation and cirrus cloud microphysics. Broadband, infrared absorption coefficients (σ) were also computed and

found to exhibit a similar temperature dependence as data recently presented by other authors.

The horizontal variabilities in the shortwave and infrared properties of these cirrus systems were explored with frequency distributions of simple radiation parameters derived from the aircraft data. The range of variation in the shortwave properties were found to be similar to the observed range in the infrared. Good correlation was found between the shortwave albedo (ρ) and upward effective emittance ($\epsilon^* \uparrow$). A scatter plot of these two parameters agreed well with theoretical calculations assuming an asymmetry parameter of 0.7. The frequency distributions of $\epsilon^* \uparrow$ were essentially bimodal in every case owing to variations in the scene below the cirrus decks (land vs. solid and broken undercast). It was also discovered that while the downward effective emittance ($\epsilon^* \downarrow$) was found to range from about 0.4 to 0.8, the shortwave effective extinction ranged from 0 to 0.45. Although the variability in the infrared properties of cirrus have been characterized in terms of the effective emittance, this should be representative of the variabilities in ϵ_{cld} since these two parameters were found to be linearly correlated.

Finally, the current state of cirrus radiation parameterizations was briefly assessed and there appears to be sufficient observational evidence to support the initial development of parameterization schemes for general circulation and climate models. Such a scheme has been invoked in the UCLA/GLA GCM and is fairly consistent with the FIRE data presented above.

REFERENCES

Abakumova, G. M., P. P. Anikin, T. V. Yevnevich, E. M. Feigelson, I. A. Gorchakova, L. V. Kravets, Ye. I. Nezval', A. G. Petrushin, T. A. Tarasova and T. A. Tochilkina, 1989: The geometrical, optical and radiative properties of cirrus clouds. *Atmos. Sci. Pap. No. 456*, Colorado State University, Ft. Collins, 100 pp. [Available from the Department of Atmospheric Science, Colorado State University, Fort Collins, CO 80523].

Ackerman, S. A., and S. K. Cox, 1981: Aircraft observations of the shortwave fractional absorptance of non-homogeneous clouds. *J. Appl. Meteor.*, **20**, 128-133.

Ackerman, S. A., W. L. Smith, J. Spinhirne and H. E. Revercomb, 1989: The 27-28 October 1986 FIRE cirrus case study: Spectral properties of cirrus clouds in the 8-12 μm window. Submitted to *Mon. Wea. Rev.*

Albrecht, B. A., M. Poellot and S. K. Cox, 1974: Pyrgeometer measurements from aircraft. *Rev. Sci. Instrum.*, **45**, 33-38.

Albrecht, B., and S. K. Cox, 1976: Radiation data reduction procedures for Sabreliner, C-10 and DC-6 aircraft during GARP Atlantic Tropical Experiment. *Atmos. Sci. Pap. No. 244*, Colorado State University, Ft. Collins, 100 pp. [Available from the Department of Atmospheric Science, Colorado State University, Fort Collins, CO 80523].

Albrecht, B., and S. K. Cox, 1977: Procedures for improving pyrgeometer performance. *J. Appl. Meteor.*, **16**, 188-197.

Bretherton, F.P., and V. E. Suomi, 1983: First International Satellite Cloud Climatology Project Regional Experiment (FIRE) Research Plan, 76 pp. [Available from the National Climatic Program Office, Rm. 108, 11400 Rockville Pike, Rockville, MD., 20852.]

Cox, S. K., 1971: Cirrus clouds and climate. *J. Atmos. Sci.*, **28**, 1513-1515.

Cox, S. K. and K. T. Griffith, 1979: Estimates of radiative divergence during phase III of the GARP Atlantic Tropical Experiment: Part I. Methodology. *J. Atmos. Sci.*, **36**, 575-585.

Cox, S. K., D. McDougal, D. Randall and R. Schiffer, 1987: FIRE: The first ISCCP regional experiment. *Bull. Amer. Meteor. Soc.*, **67**, 114-118.

Griffith, K.T. and S.K. Cox, 1977: Infrared radiative properties of tropical cirrus clouds inferred from aircraft measurements. *Atmos. Sci. Pap. No. 269*, Colorado State University, Ft. Collins [Available from the Department of Atmospheric Science, Colorado State University, Fort Collins, CO 80523]

Griffith, K., S. K. Cox, and R. G. Knollenberg, 1980: Infrared radiative properties of tropical cirrus clouds inferred from aircraft measurements. *J. Atmos. Sci.*, **37**, 1077-1087.

Harshvardhan and D. A. Randall, 1985: Comments on "The parameterization of radiation for numerical prediction and climate models". *Mon. Wea. Rev.*, **113**, 1832-1833.

Herman, B. M., 1962: Infrared absorption, scattering, and total attenuation cross-sections for water spheres. *Q. J. R. Meteorol. Soc.*, **88**, 143-150.

Hein, P. F., S. K. Cox and C. M. Johnson-Pasqua, 1987: The Sabreliner data set of the FIRE Cirrus IFO: FIRE Series No. 1. *Atmos. Sci. Pap. No. 418*, Colorado State University, Ft. Collins, 52 pp. [Available from the Department of Atmospheric Science, Colorado State University, Fort Collins, CO 80523]

Heymsfield, A. J. and C. M. R. Platt, 1984: A parameterization of the particle size spectrum of ice clouds in terms of the ambient temperature and the ice water content. *J. Atmos. Sci,*, **41**, 846.

Heymsfield, A. J. and K. M. Miller, 1989: The 27-28 October 1986 FIRE IFO cirrus case study: Cloud structure and composition from in-situ measurements. Submitted to *Mon. Wea. Rev.*

Hunt, G. E., 1973: Radiative properties of terrestrial clouds at visible and infra-red thermal window wavelengths. *Quart. J. Roy. Meteorol. Soc.*, **99**, 346-369.

Liou, K-N., 1974: On the radiative properties of cirrus in the window region and their influence on remote sensing of the atmosphere. *J. Atmos. Sci.* **31**, 522-532.

Liou, K-N., 1986: Review: Influence of cirrus clouds on weather and climate processes: a global perspective. *Mon. Wea. Rev.* **114**, 1167-1197.

Marwitz, J. D., 1987: Deep orographic storms over the Sierra Nevada. Part II: The precipitation process. *J. Atmos. Sci.* **44**, 174-185.

McClatchey, R., R. A. Fenn, J. E. A. Selby, F. E. Volz, and J. S. Garing, 1972: Optical properties of the atmosphere, 3rd ed. AFCRL-72-0497, Air Force Cambridge Research Labs., 107 pp.

Paltridge, C. W., and C. M. R. Platt, 1981: Aircraft measurements of solar and infrared radiation and the microphysics of cirrus clouds. *Quart. J. Roy. Meteor. Soc.*, **107**, 367-380.

Paltridge, G. W., 1974: Infrared emissivity, shortwave albedo and the microphysics of stratiform water clouds. *J. Geophys. Res.*, **79**, 4053-4058.

Pinnick, R. G., S. G. Jennings, P. Chylek and H. J. Auverman, 1979: Verification of a linear relation between IR extinction, absorption and liquid water content of fogs. *J. Amos. Sci.*, **36**, 1577-1586.

Platt, C. M. R., 1973: Lidar and radiometric observations of cirrus clouds. *J. Atmos. Sci.*, **30**, 1191-1294.

Platt, C. M. R., J. C. Scott, and A. C. Dilley, 1987. Remote sounding of high clouds. VI. Optical properties of midlatitude and tropical cirrus. *J. Atmos. Sci.*, **44**, 729-747.

Platt, C. M. R., and Harshvardhan, 1988: Temperature dependence of cirrus extinction: implications for climate feedback. *J. Geophy. Res.* **93**, 11,051-11,058.

Prabhakara, C., R. S. Fraser, G. Dalu, Man-Li C. Wu, R. J. Curran and T. Styles, 1988: Thin cirrus clouds: Seasonal distribution over oceans deduced from Nimbus-4 IRIS. *J. Appl. Meteor.*, **27**, 379-399.

Ramanathan, V., E. J. Pitcher, R. C. Malone and M. L. Blackmon, 1983: The response of a spectral general circulation model to refinements in radiative processes. *J. Amos. Sci.*, **40**, 605-630.

Randall, D. A., Harshvardhan, D. A. Dazlich and T. G. Corsetti 1989: Interactions among radiation, convection and large-scale dynamics in a general circulation model. *J. Amos. Sci.*, **46**, 1943- 1970.

Rockwood, A. A. and S. K. Cox, 1976: Satellite inferred albedo over northwestern Africa. *Atmos. Sci. Pap. No. 262*, Colorado State University, Ft. Collins, 64 pp. [Available from the Department of Atmospheric Science, Colorado State University, Fort Collins, CO 80523]

Smith, Jr., W. L., S. K. Cox and V. Glover, 1988: Temperature sensitivity of Eppley broadband radiometers. *Atmos. Sci. Pap. No. 423*, Colorado State University, Ft. Collins, 12 pp. [Available from the Department of Atmospheric Science, Colorado State University, Fort Collins, CO 80523]

Smith, Jr., W. L., P. F. Hein and S. K. Cox, 1989: The 27-28 October 1986 FIRE IFO cirrus case study: In situ observations of radiation and dynamic properties of a cirrus cloud layer. Submitted to *Mon. Wea. Rev.*

Stackhouse, P.W., Jr. A Theoretical and observational comparison of cirrus cloud radiative properties. M.S. Degree, 117 pp. Department of Atmospheric Science, Colorado State University, Ft. Collins, CO. July, 1989.

Starr, D. O'C. and S.K. Cox 1985: Cirrus clouds. Part I: A Cirrus cloud model. *J. Atmos. Sci.*, **42**, 2663-2681.

Starr, D. O'C., 1987: A cirrus cloud experiment: Intensive field observations planned for FIRE. *Bull. Amer. Meteor. Soc.*, **68**, 119-124.

Starr, D. O'C., and D. Wiley, 1989: The 27-28 October 1986 FIRE cirrus case study: Synoptic conditions. Submitted to *Mon. Wea. Rev.*.

Starr, D. O'C., and D. P. Wylie, 1988: Synoptic conditions producing cirrus during the FIRE cirrus IFO. Workshop report, FSET workshop, July, Vail, Colorado. [Available from FIRE Project Office, Mail Stop 483, NASA Langley Research Center, Hampton, VA, S-12].

Stephens, G. L., 1978: Radiation profiles in extended water clouds, II. Parameterization schemes. *J. Atmos. Sci.*, **35**, 2123-2132.

Stephens, G. L., 1980: Radiative properties of cirrus clouds in the infrared region. *J. Atmos. Sci.*, **37**, 435-446.

Stephens, G. L., 1987: On the effects of ice crystal porosity on the radiative characteristics of cirrus clouds. *J. Geophysical Res.* **92**, 3979-3984.

Stephens, G. L., 1979: Optical properties of eight water cloud types. *CSIRO Aust. Div. Atmos. Phys. Tech. Pap. No. 36*, 1-35. [Available from CSIRO, Private Bag No. 1, Mordialloc, Victoria 3195, Australia]

Stephens, G. L. and Si-Chee Tsay 1989: On the cloud absorption anomaly. Submitted to *Quart. J. Roy. Meteorol. Soc.*.

Wetherald, R. T., and S. Manabe 1988: Cloud feedback processes in a general circulation model. *J. Atmos. Sci.*, **45**, 1397- 1415.

Appendix A

FLIGHT AND DATA DESCRIPTION

The analysis presented here was conducted for four cirrus systems that were penetrated by the NCAR Sabreliner during the first Cirrus IFO in the fall of 1986. For each of these four flights, a stepped racetrack pattern was flown in order to sample the horizontal and vertical radiative, microphysical and dynamic structure of the cirrus clouds. No attempt was made to follow the cirrus as it was advected by the wind. This was due to air space restrictions and also because, in most cases, it was not visually obvious that the cirrus being advected into the region was any different than that being advected out. Two video cameras were mounted inside the aircraft to aid in scene identification and cloud top and base estimates.

Broadband, infrared (4-50μm) and shortwave (0.3-2.8μm) fluxes were obtained from measurements made by pyrgeometers and pyranometers manufactured by Eppley Laboratories Inc. For a description of these radiometers and calibration procedures, see Albrecht and Cox (1976, 1977) and Smith, Jr., *et al.,* (1988). In addition, the shortwave irradiances were corrected to a horizontal plane and normalized to common time by taking into account Sabreliner flight information (i.e. pitch, roll, and heading), as well as the sun-earth geometry (Rockwood and Cox 1976; Ackerman and Cox 1981). The microphysics data were obtained from the Particle Measuring System, Inc. (PMS) 2-D probes. These data are described by Heymsfield and Miller (1989). For a description of the Sabreliner data set, see Hein, *et al.,* (1987).

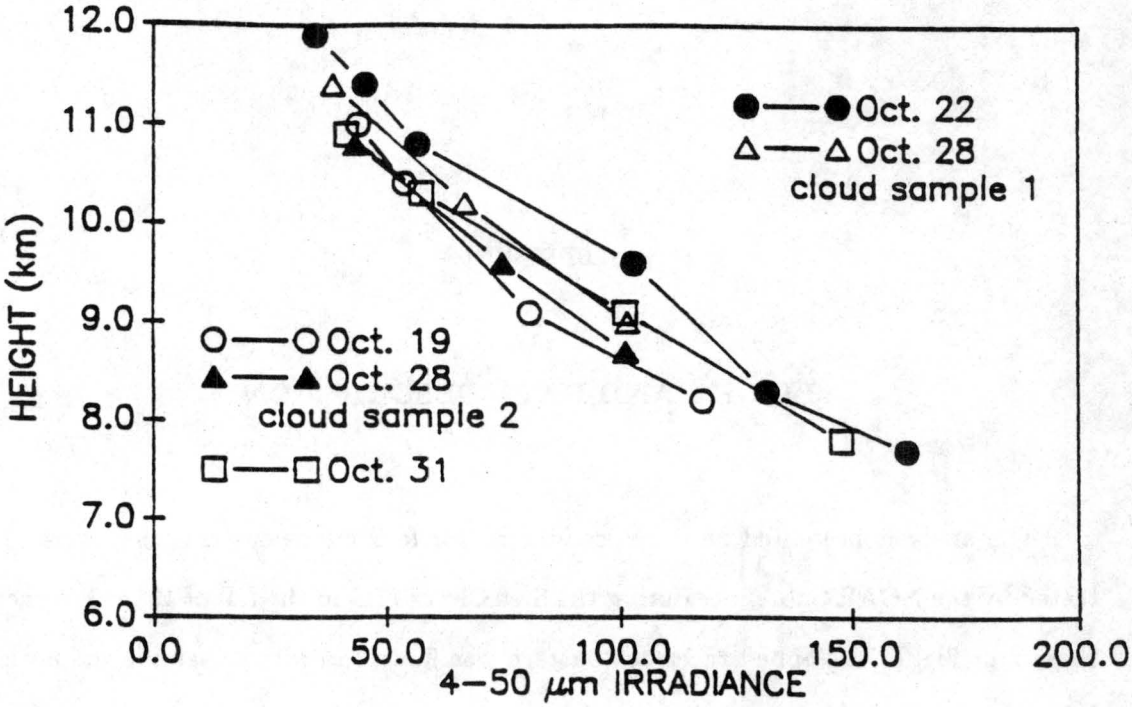

Figure A.1: Vertical profiles of downwelling 4-50 μm irradiance for five cirrus systems penetrated by the NCAR Sabreliner.

A.1 Flight Summary

A brief description of each of the four flights and the associated synoptic conditions are given below. Figs. A.1-A.10 should assist the reader in visualizing the mean vertical structure in the radiative and microphysical properties of the cirrus clouds observed from the NCAR Sabreliner. Figs. A.1 and A.2 show the measured profiles of mean downwelling 4-50 μm and 0.3- 2.8 μm irradiance for the five cirrus systems penetrated by the NCAR Sabreliner. Figs. A.3, A.5, A.7 and A.9 depict the vertical profiles of mean ice water content (IWC) and Figs. A.4, A.6, A.8 and A.10 show profiles of mean $\overline{D}_{mass}$ and D_{max}. $\overline{D}_{mass}$ is the median mass weighted ice particle dimension and D_{max} is the maximum dimension. The horizontal bars about the means represent the standard deviation in the data at each altitude.

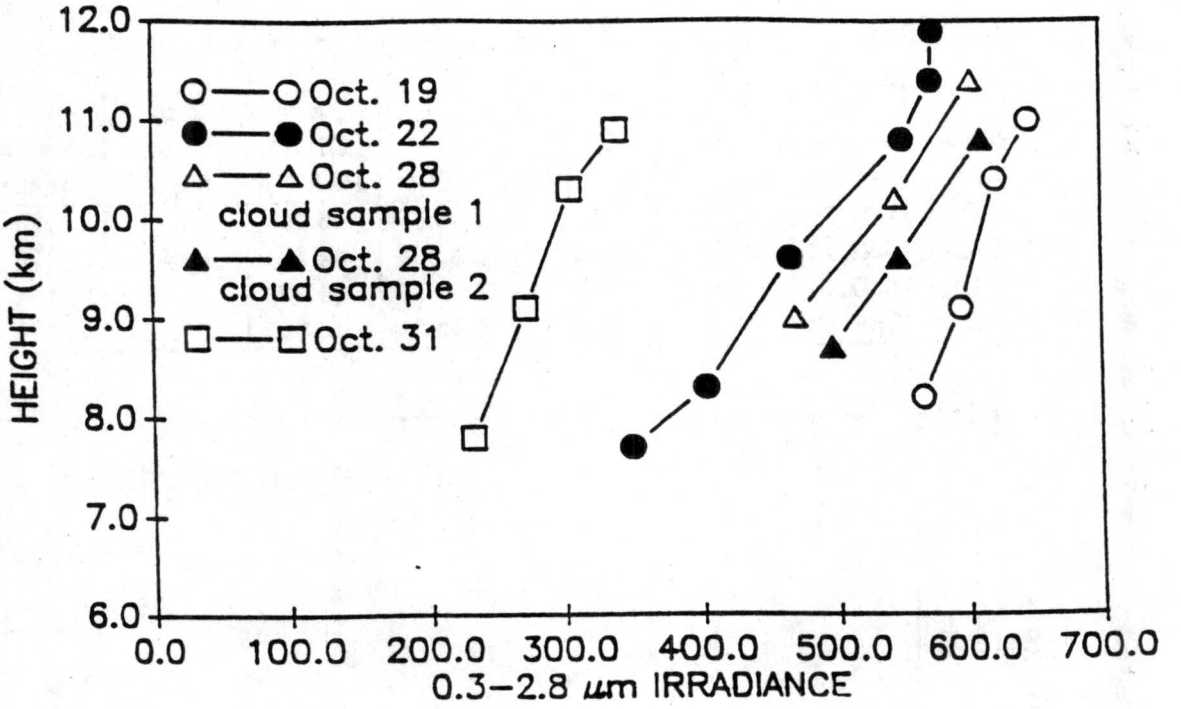

Figure A.2: Vertical profiles of downwelling 0.3-2.8 μm irradiance for five cirrus systems penetrated by the NCAR Sabreliner.

A.1.1 19 October 1986

On 19 October 1986, the Sabreliner sampled cirrus in the vicinity of Fargo, North Dakota. The cirrus sampled here developed rapidly and appeared to be associated with the passage of a weak short wave ridge emanating from a strong closed low pressure system over central Nevada. The development of this cirrus system seemed to best fit the warm front type described by Starr and Wylie (1988). Six constant altitude flight legs were flown about 60 degrees off the mean wind direction (WSW). Table A.1 lists the time, position and heading for four of these legs.

Two legs were flown further west than the other four. Profiles of mean BBSW and BBIR irradiances depicted that these data were inconsistent with the rest. For this reason, these two legs were eliminated from our analysis. Identifying the cloud top altitude was difficult. The top of a layer at about 10.4 km was evident in the videotape. However, after close inspection of the irradiance measurements and with some evidence from the videotape, it was concluded that a thin cirrus layer existed between 10.4 and 11.0 km

Table A.1: Times, positions, and headings for 19 October 1986.

Height (km)	Start Time (UTC)	Start Lat (deg N)	Start Long (deg W)	End Time (UTC)	End Lat (deg N)	End Long (deg W)	Heading (deg)
11.0	17:31:21	46.54	93.31	17:34:59	46.34	95.82	120
10.4	16:28:53	46.51	96.28	16:32:07	46.32	95.82	125
9.1	16:47:46	46.61	96.49	16:52:37	46.32	95.81	124
8.2	17:08:42	46.59	96.45	17:13:21	46.33	95.82	124

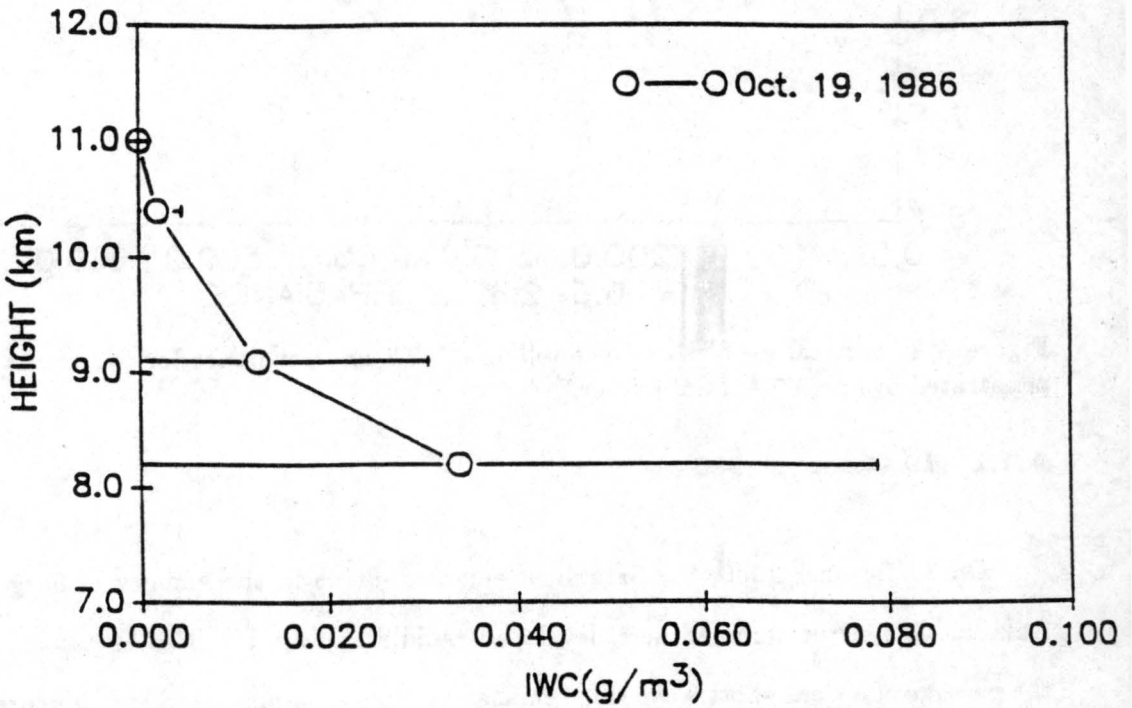

Figure A.3: Vertical profile of ice water content (IWC) through a cirrus cloud sampled on October 19, 1986.

during much of the flight. For the analysis discussed in Chapter 3, cloud top height was assumed to be 11.0 km. Cloud base was never actually penetrated but the lowest leg at 8.2 km was estimated to be within 0.5 km of the cloud base. Analysis of the videotape also revealed that the cirrus sampled on this day was very inhomogenous in comparison to the other cirrus cloud systems.

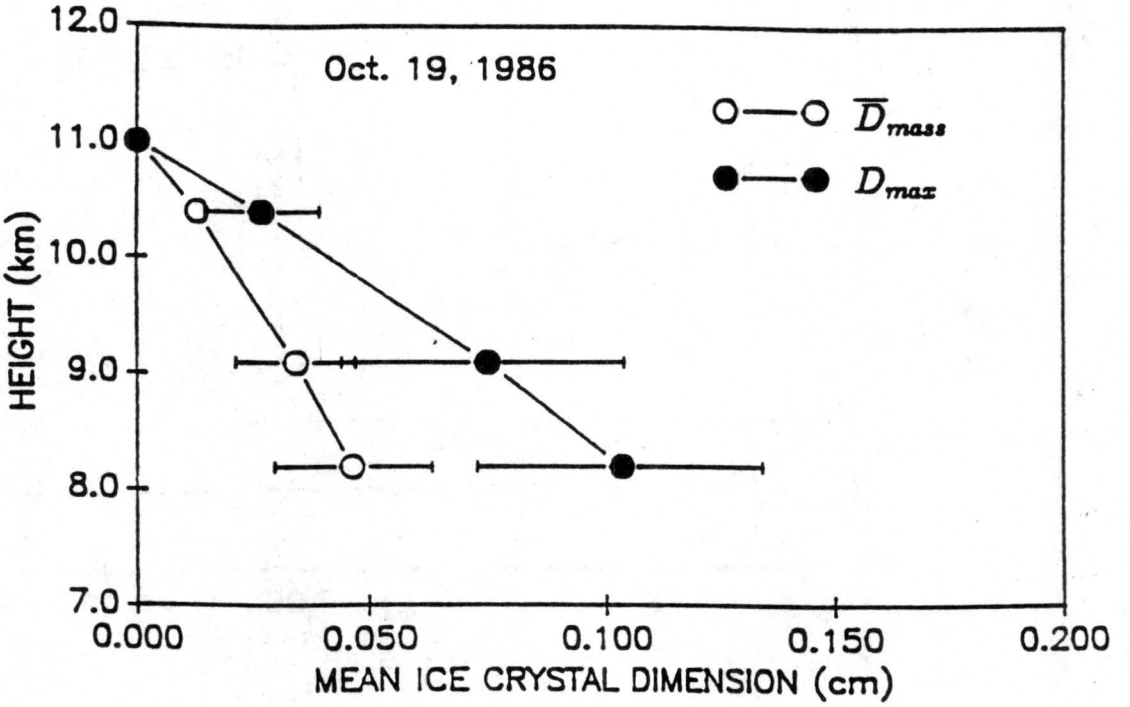

Figure A.4: Vertical profile of mean ice crystal dimension for the cirrus cloud sampled on October 19, 1986. See text for description of the parameters $\overline{D}_{mass}$ and D_{max}.

A.1.2 22 October 1986

On 22 October 1986, the Sabreliner penetrated a high cirrostratus deck over central Wisconsin with eight constant altitude flight legs along the mean wind direction (WSW). A closed low pressure system resided over southwestern Nebraska. The cirrus deck sampled on this day was observed in the vicinity of the exit region ridge of this closed low and has been classified as "closed low cirrus" (Starr and Wylie, 1988). Two of the flight legs were eliminated due to cloud sampling problems. In both cases, the shortwave (infrared) mean irradiances were small (large) compared to the other data comprising a vertical profile. The apparent profile appeared jagged and unrealistic. When these two legs were removed, the resulting profiles were rather smooth and more realistic. It is uncertain what conditions were responsible for this irregularity in the measured vertical irradiance profiles and we can only speculate that optically denser cloud elements had advected into the region being sampled by the Sabreliner or that there was significant ice crystal growth overhead. Another possibility is that a cirrus deck formed or was advected into the region

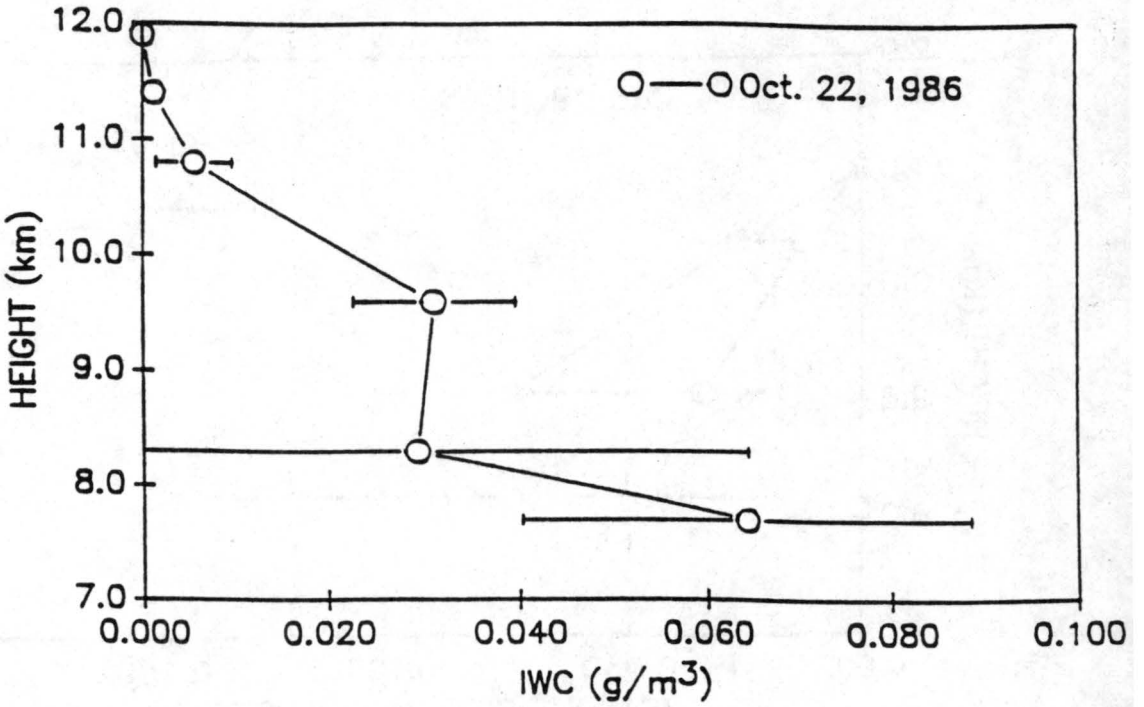

Figure A.5: Same as A.3 but for October 22, 1986.

that was higher than the observed cloud top height at 11.8 km. This seems less likely since the cloud top was very close to the tropopause. Table A.2 lists the time, position and heading for the six flight legs used in our analysis.

Table A.2: Times, positions, and headings for 22 October 1986.

Height (km)	Start Time (UTC)	Start Lat (deg N)	Start Long (deg W)	End Time (UTC)	End Lat (deg N)	End Long (deg W)	Heading (deg)
11.9	19:34:26	44.04	88.94	19:38:27	43.86	89.42	242
11.4	19:42:39	43.82	88.93	19:44:09	43.93	88.71	56
10.8	19:50:30	44.06	88.92	19:52:18	43.99	89.12	243
9.6	20:07:49	44.08	88.83	20:09:51	43.98	89.05	240
8.3	20:21:15	43.98	89.05	20:23:00	43.92	89.25	247
7.7	20:30:05	43.86	88.87	20:32:05	43.96	88.63	56

A.1.3 28 October 1986

Observations of radiation and dynamic properties of a cirrus cloud layer penetrated by the NCAR Sabreliner on 28 October 1986 have been described by Smith Jr., *et al.*, (1989). This case was selected to undergo detailed investigation by various members of

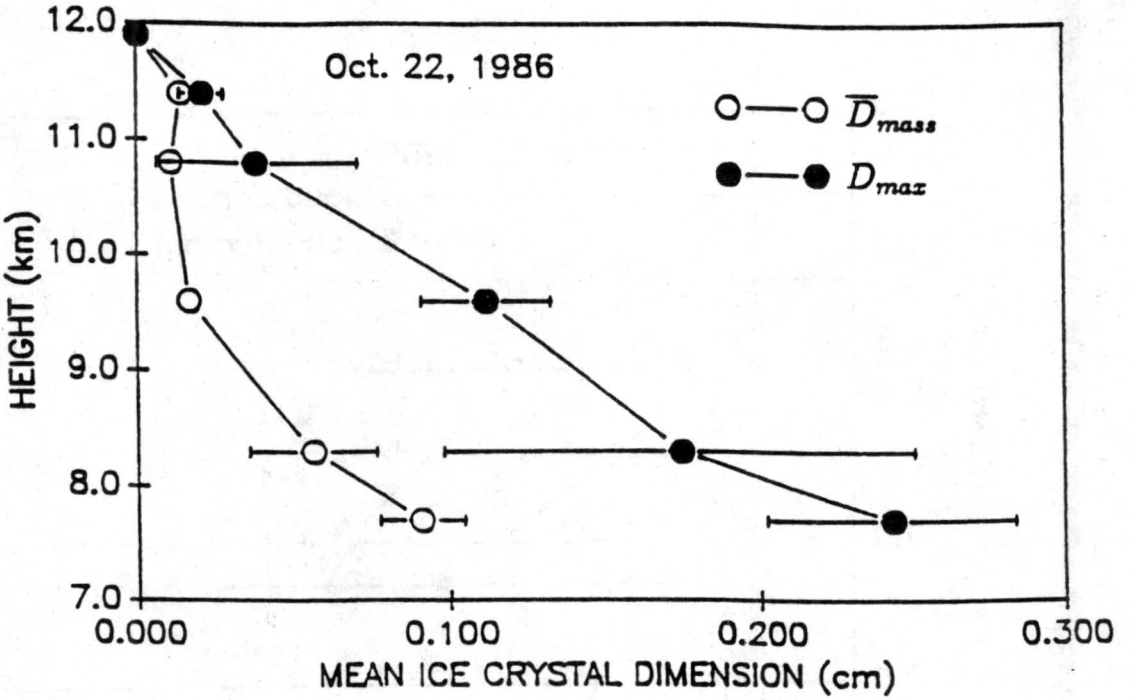

Figure A.6: Same as A.4 but for October 22, 1986.

the Fire Science Experiment Team (FSET) and others. The results of these investigations are to appear collectively in an issue of Monthly Weather Review. Some of the results of Smith Jr., *et al.*, (1989) are repeated here for coherence and because they warrant an intercomparison with the results of the other three cases. For a detailed description of the synoptic conditions on 28 October 1986, see Starr and Wylie (1989). Tables A.3 and A.4 list the time, position and heading for Cloud Sample 1 and Cloud Sample 2.

Table A.3: Times, positions, and headings for Cloud Sample 1 on 28 October 1986.

Height (km)	Start Time (UTC)	Start Lat (deg N)	Start Long (deg W)	End Time (UTC)	End Lat (deg N)	End Long (deg W)	Heading (deg)
11.4	15:45:48	44.45	87.89	15:48:58	44.29	87.41	120
10.2	16:00:56	44.45	87.89	16:04:31	44.27	87.36	119
9.0	16:16:47	44.44	87.93	16:20:41	44.28	87.36	113

A.1.4 31 October 1986

On 31 October 1986, the NCAR Sabreliner penetrated "jet stream" cirrus with six constant altitude flight legs along the mean wind direction (WNW). A cold front extended

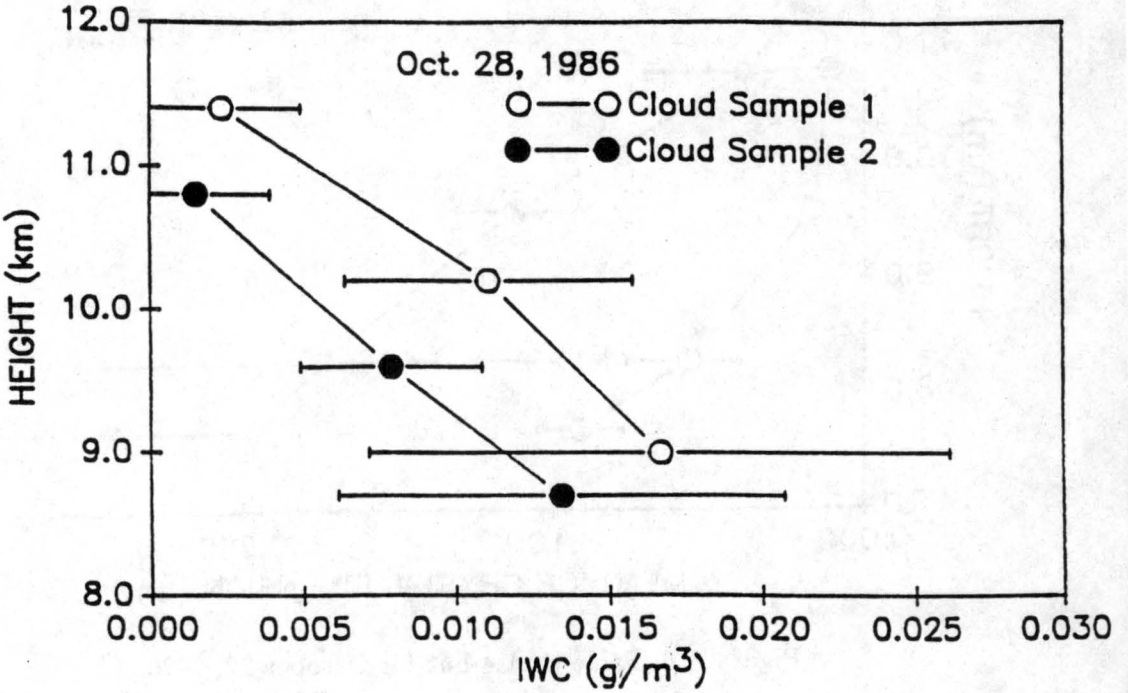

Figure A.7: Same as A.3 but for October 28, 1986.

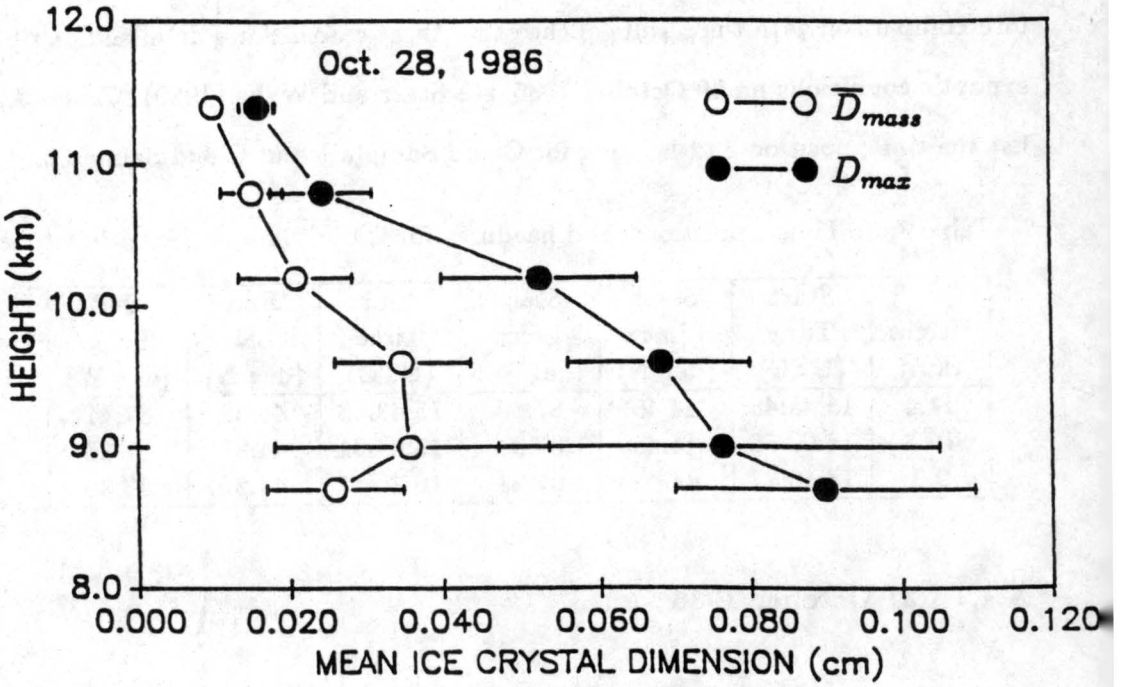

Figure A.8: Same as A.4 but for October 28, 1986.

Table A.4: Times, positions, and headings for Cloud Sample 2 on 28 October 1986.

Height (km)	Start Time (UTC)	Start Lat (deg N)	Start Long (deg W)	End Time (UTC)	End Lat (deg N)	End Long (deg W)	Heading (deg)
10.8	15:53:20	44.54	87.39	15:57:17	44.86	87.91	288
9.6	16:07:45	44.45	87.21	16:13:30	44.65	87.93	289
8.7	16:24:44	44.48	87.36	16:30:34	44.52	88.11	275

from a surface low pressure system in central Ontario through Minnesota and Wisconsin, just west of the IFO region. The cirrus observed on this day has been classified as "cold front cirrus" by Starr and Wylie (1988). This type of cirrus has also been described as "baroclinic zone" cirrus and "jet stream" cirrus. A moderate jet was associated with the cirrus sampled by the Sabreliner as measured wind speeds were as large as 50 m/s in the top of the cirrus layer. Two of the five flight legs within the cloud were flown on the south side of a racetrack pattern while the other three legs were flown on the north side (about 35 km away). Upon inspection of the radiation and cloud microphysics data, it became apparent that the cloud being sampled on the south side of the racetrack was optically thinner than that being sampled on the north side and so these data have been eliminated from our analysis. Table A.5 lists the time, position and heading for the three legs flown in cloud and a fourth flown at the cloud top height of 10.9 km. Cloud base was never ascertained as the cirrus seemed to extend down to an altostratus deck at about 7.5 km.

Table A.5: Times, positions, and headings for 31 October 1986.

Height (km)	Start Time (UTC)	Start Lat (deg N)	Start Long (deg W)	End Time (UTC)	End Lat (deg N)	End Long (deg W)	Heading (deg)
10.9	20:34:52	46.09	87.86	20:37:21	46.26	87.47	56
10.3	20:41:15	46.37	87.65	20:46:15	46.15	88.12	236
9.1	20:56:51	46.36	87.56	21:02:36	46.13	88.13	240
7.8	21:15:20	46.26	87.58	21:18:44	46.03	87.80	220

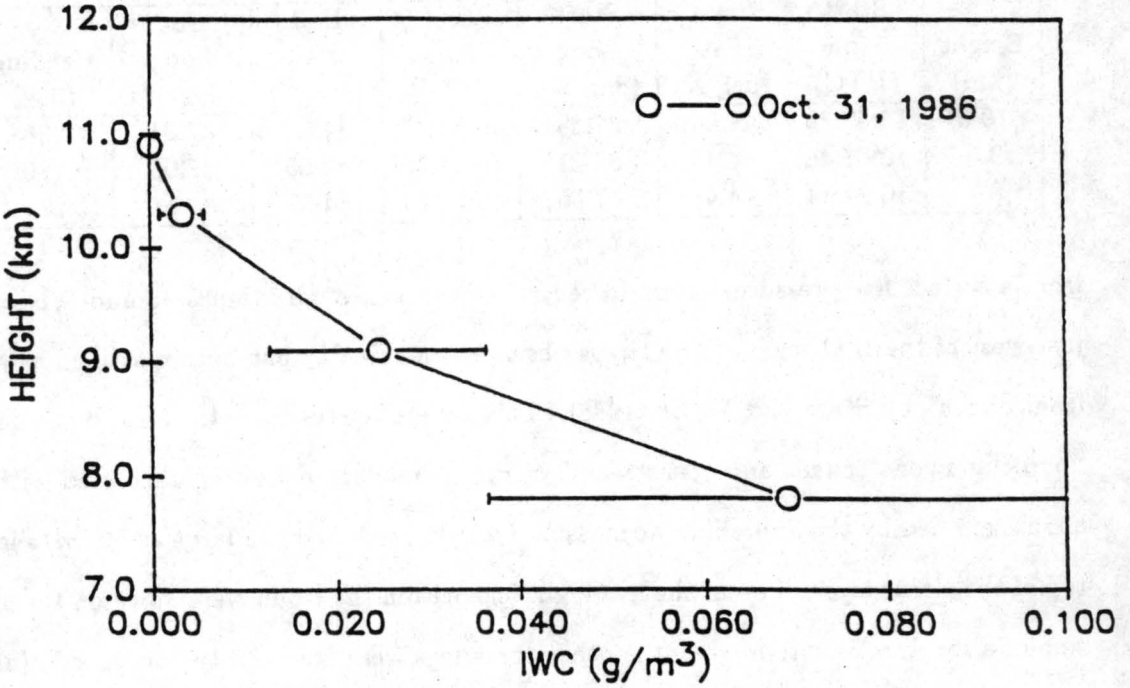

Figure A.9: Same as A.3 but for October 31, 1986.

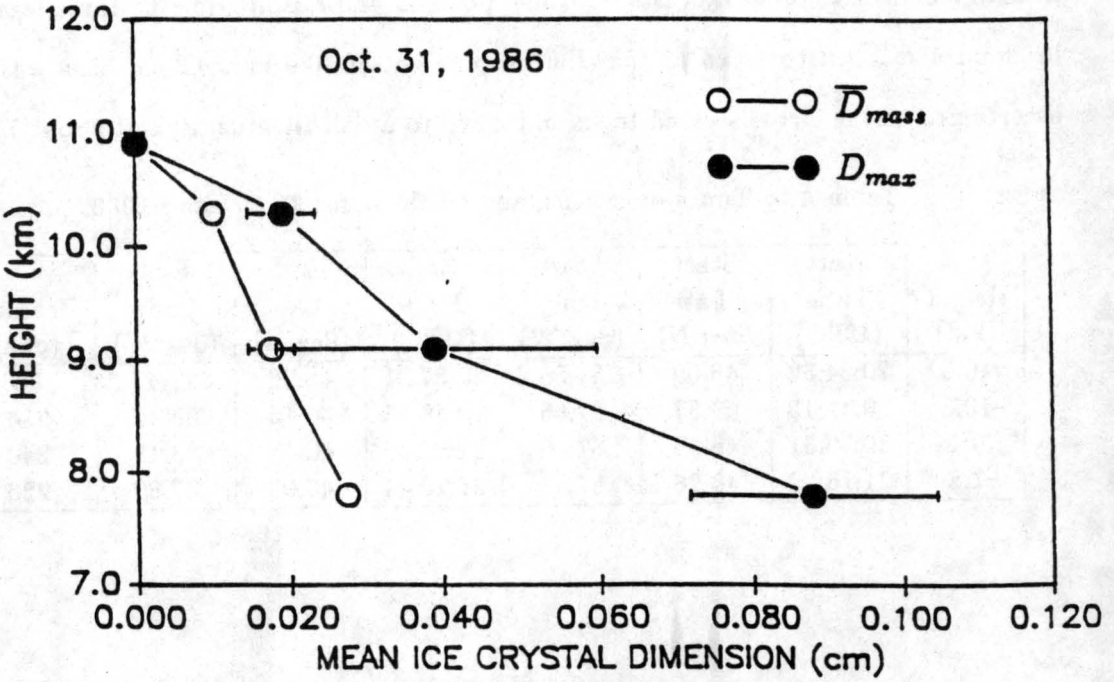

Figure A.10: Same as A.4 but for October 31, 1986.